# Glucocorticoids drive diurnal oscillations in T cell distribution and responses by inducing interleukin-7 receptor and CXCR4

**Akihiro Shimba[1,2], Guangwei Cui[1], Shizue Tani-ichi[1,3], Makoto Ogawa[1,2], Shinya Abe[1,2], Fumie Okazaki[1,2], Satsuki Kitano[4], Hitoshi Miyachi[4], Hisakata Yamada[5], Takahiro Hara[1], Yasunobu Yoshikai[5], Takashi Nagasawa[6], Günther Schütz[7], and Koichi Ikuta[1,8,*]**

[1]Laboratory of Immune Regulation, Department of Virus Research, Institute for Frontier Life and Medical Sciences, Kyoto University, Kyoto 606-8507, Japan; [2]Graduate School of Medicine, Kyoto University, Kyoto 606-8501, Japan; [3]Laboratory of Biological Chemistry, Human Health Sciences, Graduate School of Medicine, Kyoto University, Kyoto 606-8507, Japan; [4]Reproductive Engineering Team, Institute for Frontier Life and Medical Sciences, Kyoto University, Kyoto 606-8507, Japan; [5]Division of Host Defense, Network Center for Infectious Diseases, Medical Institute of Bioregulation, Kyushu University, Fukuoka 812-8582, Japan; [6]Laboratory of Stem Cell Biology and Developmental Immunology, Graduate School of Frontier Biosciences and Graduate School of Medicine, Osaka University, Osaka 565-0871, Japan; [7]Department of Molecular Biology of the Cell I, German Cancer Research Center, Heidelberg 69120, Germany; [8]Lead Contact.

*Correspondence: ikuta.koichi.6c@kyoto-u.ac.jp

**SUMMARY**

Glucocorticoids are steroid hormones with strong anti-inflammatory and immunosuppressive effects that are produced in a diurnal fashion. Although glucocorticoids have the potential to induce interleukin-7 receptor (IL-7R) expression in T cells, whether they control T cell homeostasis and responses at physiological concentrations remains unclear. We found that glucocorticoid receptor signaling induces IL-7R expression in mouse T cells by binding to an enhancer of the IL-7Rα locus, with a peak at midnight and a trough at midday. This diurnal induction of IL-7R supported the survival of T cells and their redistribution between lymph nodes, spleen, and blood by controlling expression of the chemokine receptor CXCR4. In mice, T cell accumulation in the spleen at night enhanced immune responses against soluble antigens and systemic bacterial infection. Our results reveal the immunoenhancing role of glucocorticoids in adaptive immunity and provide insight into how immune function is regulated by the diurnal rhythm.

Keywords: glucocorticoid, interleukin-7, diurnal rhythm, T cell, CXCR4

## INTRODUCTION

Glucocorticoids are a group of steroid hormones that contribute to diverse biological processes, including glucose metabolism, cognition, and stress resistance. They also have strong anti-inflammatory and immunosuppressive effects, and are widely used in clinical practice. Glucocorticoids are produced by the adrenal cortex in response to adrenocorticotropic hormone in a diurnal fashion. In human, blood glucocorticoids levels peak in the morning and fall over the course of the day and the first part of the night. In nocturnal animals, such as mice, this circadian fluctuation is reversed. Glucocorticoids exert their functions by binding to glucocorticoid receptor (GR) in the cytoplasm. The GR is then transmitted to the nucleus, where it acts as a transcription factor by binding to glucocorticoid response elements (GREs) of target genes. GRs suppresses expression of inflammatory cytokines both directly, by binding to the corresponding gene loci, and indirectly, by binding to transcription factors such as AP-1 and NF-κB (Ashwell et al., 2000). Glucocorticoids induce apoptosis of $CD4^{+}CD8^{+}$ immature thymocytes (Screpanti et al., 1989). Nevertheless, T-cell development is not impaired in GR-deficient mice (*Nr3c1*$^{-/-}$) (Purton et al., 2000). Hence, the physiological functions of glucocorticoids in the immune system remain unclear.

Glucocorticoids have a direct link with the immune system; for example, they induce the expression of IL-7 receptor α-chain (IL-7Rα) in T cells (Franchimont et al., 2002). IL-7, a cytokine critical for development and maintenance of the immune system (Mazzucchelli and Durum, 2007), is a member of common γ-chain cytokine family. By activating the transcription factor signal transducer and activator of transcription (STAT) 5 and phosphatidylinositol 3-kinase, IL-7R signaling promotes proliferation, survival, and differentiation of T cells. We previously reported that a GR binds to a GRE in an enhancer of the IL-7Rα locus and activates its transcription (Lee et al., 2005). Indeed, targeted deletion of

the IL-7Rα enhancer results in reduced expression of IL-7R and impaired survival and response of peripheral T cells (Abe et al., 2015). Furthermore, IL-7Rα enhancer–deficient mice totally lack IL-7R induction by glucocorticoids in T cells. These results suggest that glucocorticoids may promote T cell homeostasis by inducing IL-7R expression.

The circadian rhythm exerts a considerable influence on the immune system. Adrenergic neural signals regulate the adaptive immune response via diurnal lymphocyte recirculation in lymph nodes (Suzuki et al., 2016). More directly, the lymphocyte clock gene *Arntl* controls trafficking through lymph nodes and immune responses by regulating chemokine receptor CCR7 and sphingosine-1-phosphate receptor 1 (S1PR1) expression (Druzd et al., 2017). Because of their diurnal production, glucocorticoids are important circadian mediators. For example, glucocorticoids regulate the expression of intrinsic clock genes such as *Per2* and *Nfil3* and drive circadian change throughout the body (So et al., 2009). In addition, glucocorticoids control circadian changes of chemokine CXCL5 expression in pulmonary epithelial cells under inflammatory conditions and neutrophil recruitment (Gibbs et al., 2014), implying that glucocorticoids play roles in innate and adaptive immune responses.

To investigate whether glucocorticoids regulate T cell homeostasis and function in a diurnal rhythm by regulating IL-7R expression, we analyzed IL-7Rα enhancer GRE mutant and T cell specific GR-deficient mice ($Nr3c1^{fl/fl}Cd4\text{-cre}^{+}$). We found that IL-7R is induced by GRs in a diurnal rhythm, which supports T cell survival and recruitment to lymph nodes, spleen, and Peyer's patches via CXCR4 expression. Moreover, the diurnal change in T cell distribution enhanced immune responses at night in mice. Collectively, our results demonstrate that adaptive immunity is under diurnal control by glucocorticoids, unveiling a new link between the endocrine and immune systems.

## RESULTS

### GRs Regulate Diurnal Changes in IL-7R Expression and Numbers of T Cells in Lymphoid Organs

To determine whether glucocorticoids regulate T cell homeostasis and activity *in vivo*, we examined IL-7R expression in T cell-specific GR-deficient (*Nr3c1*$^{fl/fl}$*Cd4*-cre$^{+}$) mice (Figure S1A). IL-7R expression was unchanged in most thymocytes, except for thymic regulatory T (Treg) cells, which exhibited reduced IL-7R expression (Figures S1B and S1C) but underwent normal development (Figures S1D–H). In the periphery, IL-7R expression was reduced in *Nr3c1*$^{fl/fl}$*Cd4*-cre$^{+}$ T cells (Figure 1A). Moreover, the reduction in IL-7R was observed only at night (Figure 1B). IL-7R expression changed in a diurnal fashion, with a peak at zeitgeber time (ZT, 24 hour light/dark cycle defining light on as time 0) 16 (night timepoint) and a nadir at ZT4 (day time point) in control mice, but was unchanged throughout the day in *Nr3c1*$^{fl/fl}$*Cd4*-cre$^{+}$ mice (Figure 1C). This change is likely to follow diurnal fluctuations in glucocorticoid levels (Gibbs et al., 2014). Diurnal variation of IL-7R expression was regulated at the mRNA level, and was lost in *Nr3c1*$^{fl/fl}$*Cd4*-cre$^{+}$ mice (Figure 1D), indicating that GRs regulate the diurnal rhythm of IL-7R expression in peripheral T cells. These results suggest that GRs might control diurnal changes in T cell functions.

To explore this possibility, we analyzed T cell numbers in peripheral lymphoid organs during the day. Circulating lymphocyte numbers fluctuate in human peripheral blood, rising at night and falling in daytime (Haus and Smolensky, 1999). In blood of control mice, absolute numbers of CD4$^{+}$ T, CD8$^{+}$ T, and Treg cells fluctuated, with a peak at ZT4 and a nadir at ZT16 (Figure 1E). By contrast, T cell counts in blood were lower in *Nr3c1*$^{fl/fl}$*Cd4*-cre$^{+}$ mice than in controls, and the difference between day and night was lost. Due to the diurnal change of T cell numbers in blood, we hypothesized that T cells recirculate between lymphoid

tissue and blood during the day. Indeed, the T cell count in lymph nodes exhibited a diurnal fluctuation with a peak at ZT12 and a nadir at ZT0, and this fluctuation was lost in *Nr3c1*$^{fl/fl}$*Cd4*-cre$^{+}$ mice (Figure 1F), consistent with a previous report (Druzd et al., 2017). In the spleen and Peyer's patches of control mice, T cell numbers exhibited the changes opposite to the blood, with a peak at ZT16 and a nadir at ZT4, and again this fluctuation was lost in *Nr3c1*$^{fl/fl}$*Cd4*-cre$^{+}$ mice (Figures 1G and 1H). These results suggest that GRs control T cell distribution between lymphoid organs and peripheral blood.

**GRs Regulate IL-7R Upregulation by Binding to GR Motifs in IL-7R Enhancer in vivo**

Previously, we showed that GRs regulate IL-7R expression through an enhancer of the IL-7Rα locus, conserved non-coding sequence (CNS)-1 (Abe et al., 2015). To determine whether GR directly regulates IL-7R expression *in vivo*, we generated mice harboring point mutations in one or both of two glucocorticoid response elements (GREs) in the IL-7Rα enhancer (Figures S2A–S2C). IL-7R expression was reduced in thymic Treg and peripheral T cells, but not in other thymocyte subsets, in IL7R-CNS1-GRE mutant mice (Figures 2A, S2D–S2F, and S3A–S3D). *Il7r*$^{CNS1.GRE1m/1m}$ (GRE1m) and *Il7r*$^{CNS1.GRE2m/2m}$ (GRE2m) mice, with mutations in single motifs, had reduced levels of *Il7r* mRNA and cell-surface IL-7R, whereas *Il7r*$^{CNS1.GRE12m/12m}$ (GRE12m) mice with mutations in both motifs exhibited more severe reductions. We then performed flow cytometry to further confirm the change in IL-7R expression on T cells during the day. IL-7R expression changed in a diurnal fashion with a peak at ZT16 and a nadir at ZT4 in control mice, but was unchanged throughout the day in GRE12m mice (Figure 2B). The levels of IL-7Rα mRNA also exhibited a similar diurnal change (Figure 2C). Next, we performed a chromatin immunoprecipitation (ChIP) assay to investigate whether GR binds to the CNS-1 in a diurnal fashion. Specific GR binding was observed only at night in T cells of WT mice, but this binding was completely lost in T cells

of GRE12m mice (Figure 2D).

Next, we sought to elucidate the function of GR-induced IL-7R *in vivo*. The phenotype of GRE12m mice was similar to that of *Nr3c1*$^{fl/fl}$*Cd4*-cre$^{+}$ mice, i.e., they lacked the diurnal redistribution of T cells between lymphoid tissues and peripheral blood (Figures 2E–2H). To determine whether IL-7R controls the diurnal redistribution of T cells, we analyzed T cell-specific IL-7R–deficient (*Il7r*$^{fl/fl}$*Cd4*-cre$^{+}$) mice. Although these mice exhibited a severe reduction in T cell numbers relative to control mice, the diurnal redistribution of T cells was lost (Figures S3E–S3G). These findings confirmed the previous study showing that GRs upregulate IL-7R expression by binding directly to the GRE in the IL-7Rα enhancer. Furthermore, these results suggest that GR-induced IL-7R expression regulates the diurnal change in T cell distribution between lymphoid tissues and peripheral blood.

**GRs Regulate T Cell Survival through IL-7R and Bcl2 Expression**

To assess whether the reduction of IL-7R affects T cell survival, we first cultured naive T cells with IL-7 for 6 days. IL-7 rescued fewer T cells in *Nr3c1*$^{fl/fl}$*Cd4*-cre$^{+}$ and GRE12m mice than in control mice (Figures S4A and S4B). To determine whether T cell survival was impaired *in vivo*, we labeled CD45.1$^{+}$ (control) and CD45.2$^{+}$ (*Nr3c1*$^{fl/fl}$*Cd4*-cre$^{+}$ or GRE12m) naive CD4 T cells with CFSE, mixed them, and transferred them into CD45.2$^{+}$ C57BL/6 mice. After 8 days, we compared the frequencies of T cells in spleen, lymph nodes, and peripheral blood between control and GRE12m mice. GRE12m T cells were less abundant than control T cells (Figures S4C and S4D). Furthermore, the phenotype of *Nr3c1*$^{fl/fl}$*Cd4*-cre$^{+}$ T cells was more severe than that of GRE12m T cells. Next, to determine whether T cells die at higher rates during the daytime, we compared levels of activated caspase 3, an indicator of cell death, in freshly isolated naïve CD4$^{+}$ T cells. CD4$^{+}$ T cells of control mice contained higher levels of

activated caspase 3 in the daytime than at night (Figure S4E). We then analyzed the expression of anti-apoptotic factors, Bcl2 and BclxL. *Nr3c1*$^{fl/fl}$*Cd4*-cre$^{+}$ mice expressed reduced levels of Bcl2 and BclxL in peripheral T cells and thymocytes (Figures S4F–S4H), whereas GRE12m mice did not (Figures S4I–S4K). These results suggest that GR supports T cell survival by both IL-7R–dependent and –independent pathways. Moreover, the data suggest that impaired T cell survival might play some role in the impaired T cell oscillations in the GRE12m mice. In addition, although the expression of Bcl2 and BclxL was reduced in the thymocytes of *Nr3c1*$^{fl/fl}$*Cd4*-cre$^{+}$ mice, their cell numbers were unchanged (Figure S1D–H).

**GRs and IL-7R Regulate the Diurnal Change of T Cell Distribution by Inducing CXCR4 Expression**

We next sought to elucidate the mechanism controlling the diurnal redistribution of T cells. In light of previous reports that CXCR4 is induced by glucocorticoids and IL-7 (Dimitrov et al., 2009; Jourdan et al., 2000), we monitored expression of two chemokine receptors, CXCR4 and CCR7, on naïve T cells. CCR7 expression was unchanged in *Nr3c1*$^{fl/fl}$*Cd4*-cre$^{+}$ mice relative to control mice (Figure S5A). Levels of CXCR4 protein and mRNA were high at night and low in the daytime in CD4$^{+}$ and CD8$^{+}$ T cells of control mice (Figures 3A–3F). By contrast, nighttime levels of CXCR4 mRNA were reduced in *Nr3c1*$^{fl/fl}$*Cd4*-cre$^{+}$ and GRE12m mice, and the diurnal variation in CXCR4 expression was lost in *Nr3c1*$^{fl/fl}$*Cd4*-cre$^{+}$ and GRE12m mice. To determine whether the diurnal change in CXCR4 expression influences the migration of T cells, we performed Transwell migration assays with chemokine CXCL12. In control mice, T cells isolated at night migrated more efficiently than those isolated in the daytime (Figures 3G and 3H), but this difference was abolished in *Nr3c1*$^{fl/fl}$*Cd4*-cre$^{+}$ and GRE12m mice. These results suggest that CXCR4 upregulation might cause T cell homing to

the spleen at night.

To determine whether T cell homing to spleen is impaired in mutant mice, we mixed CD45.1$^+$ (control) and CD45.2$^+$ (*Nr3c1*$^{fl/fl}$*Cd4*-cre$^+$ or GRE12m) CD4$^+$ T cells, labeled them with CFSE, and transferred them into recipient mice at daytime or night. When T cells were transferred at night the frequency of mutant T cells in spleen was reduced relative to control T cells, whereas their frequency in peripheral blood was elevated (Figures 3I and 3J); this effect was not observed when the cells were transferred at daytime. Next, to assess whether CXCR4 controls T cell redistribution, we analyzed T cell-specific CXCR4-deficient (*Cxcr4*$^{fl/fl}$*Cd4*-cre$^+$) mice. Unlike control mice, *Cxcr4*$^{fl/fl}$*Cd4*-cre$^+$ mice lacked the diurnal change in T cell numbers in blood, lymph nodes, and spleen (Figures 3K–3M). T cell numbers in blood are kept at higher levels in *Cxcr4*$^{fl/fl}$*Cd4*-cre$^+$ mice, suggesting that the impairment of homing alone does not lead to decreased cell survival. Otherwise, there was no difference between control and *Cxcr4*$^{fl/fl}$*Cd4*-cre$^+$ T cells in terms of CD127 and Bcl2 expression or *in vivo* survival (Figures S5B–S5D). These results indicate that IL-7R induced by GRs regulates CXCR4 expression in a diurnal fashion, and that CXCR4 is critical for the diurnal change in T cell distribution between lymphoid organs and blood.

We next tested whether the administration of glucocorticoids *in vivo* induces the expression of IL-7R and CXCR4 in T cells and their accumulation in spleen. IL-7R expression was elevated in CD4$^+$ T cells 4 hr after dexamethasone injection at ZT4 (Figure S5E). Concurrently, CXCR4 was induced in CD4$^+$ T cells. The numbers of CD4$^+$ T cells were also elevated in spleen. These results demonstrate that exogenous glucocorticoids recapitulate the induction of IL-7R and CXCR4 expression and the redistribution of T cells between spleen and blood. By contrast, IL-7 administration alone, neither *in vivo* nor *in vitro*, did not change CXCR4 expression in CD4$^+$ T cells (Figures S5F and S5G), suggesting that IL-7 is required, but not sufficient, for CXCR4 expression.

**GRs Regulate T-Cell Homing to CXCL12-Producing Cells**

Because CXCR4 is important for the diurnal rhythm of T cell migration, and its expression depended on IL-7 signaling, we next investigated whether GR controls T cell migration near CXCL12- and IL-7-producing cells in spleen and Peyer's patches. In spleen, CXCL12 is strongly expressed in red pulp and a subset of vessels in the T and B cell zones (Figures 4A and 4B). As expected, donor T cells accumulated around the CXCL12-expressing area, red pulp, and vessels. On the other hand, IL-7-expressing cells were scattered in the T cell zone and around vessels (Figures 4C and 4D). T cells seemed to localize around vessels surrounded by IL-7–expressing cells in the T and B cell zones. To determine whether T cell homing is impaired in *Nr3c1*$^{fl/fl}$*Cd4*-cre$^{+}$ mice, we labeled T cells from control and *Nr3c1*$^{fl/fl}$*Cd4*-cre$^{+}$ mice with different dyes, mixed them 1:1, and transferred them into *Cxcl12*-GFP mice. T cells from control mice localized more frequently in the vicinity of CXCL12$^{+}$ cells than T cells from *Nr3c1*$^{fl/fl}$*Cd4*-cre$^{+}$ mice (Figures 4E and 4F). In Peyer's patches, we detected GFP signal in and around the T cell zone (Figures S6A and S6B). T cells from control mice tended to localize near CXCL12$^{+}$ cells around the T cell zone. In contrast to spleen, vessels in Peyer's patches were surrounded by IL-7-expressing cells, but not by CXCL12$^{+}$ cells (Figures S6B and S6C), and T cells from *Nr3c1*$^{fl/fl}$*Cd4*-cre$^{+}$ mice migrated less in Peyer's patches (Figures S6D and S6E). These results indicate that CXCR4 expression induced by GRs regulates T cell homing to CXCL12-producing cells in spleen.

**GRs Enhance IL-2 Response and T Cell Activation in a Diurnal Fashion**

Because T cell priming occurs in lymphoid tissues, we hypothesized that T cell accumulation at night might induce efficient T cell activation in spleen and Peyer's patches. Because glucocorticoids and IL-7 up-regulate IL-2 receptor $\alpha$ chain (CD25) expression (Franchimont

et al., 2002), we first analyzed T cell activation after stimulation with anti-CD3 and anti-CD28 antibodies. *Nr3c1*$^{fl/fl}$*Cd4*-cre$^{+}$ CD4$^{+}$ and CD8$^{+}$ T cells isolated at ZT4 and ZT16 exhibited impaired proliferation, whereas GRE12m T cells did not (Figures 5A and S7A). Consistently, *Nr3c1*$^{fl/fl}$*Cd4*-cre$^{+}$ T cells showed reduction in CD25 expression and STAT5 phosphorylation, whereas GRE12m T cells did not (Figures 5B, 5C, and S7B). On the other hand, IL-2 receptor β chain (CD122) expression was slightly elevated in *Nr3c1*$^{fl/fl}$*Cd4*-cre$^{+}$ T cells. These results suggest that GR signal, independently of IL-7R expression, controls the proliferation of T cells after T cell receptor (TCR) stimulation. Next, we infected control and *Nr3c1*$^{fl/fl}$*Cd4*-cre$^{+}$ mice with *Listeria monocytogenes* expressing ovalbumin (OVA) and analyzed OVA-specific CD8$^{+}$ T cells. In control mice, the percentages and cell numbers of OVA-specific CD8$^{+}$ T cells were higher when mice were both infected and analyzed at night than when the manipulations were performed during the daytime (Figures 5D and 5E). By contrast, *Nr3c1*$^{fl/fl}$*Cd4*-cre$^{+}$ mice had reduced numbers of OVA-specific CD8$^{+}$ T cells, with a less prominent diurnal change. Moreover, GRE12m mice showed similar phenotype to *Nr3c1*$^{fl/fl}$*Cd4*-cre$^{+}$ mice (Figures 5F and 5G), even though T cell proliferation after TCR stimulation was not impaired. These results indicate that glucocorticoids enhance the responsiveness of CD8$^{+}$ T cells on a per-cell basis at night, in addition to increasing their absolute cell numbers.

**GRs Control Differentiation of Th Subsets and Immune Response of B Cells**

Because glucocorticoids influence type1 helper T (Th1) and Th2 cell balance (Elenkov, 2004), we next analyzed the differentiation of naive CD4$^{+}$ T cells into Th1 and Th2 cells. Differentiation of interferon (IFN)-γ–producing cells was elevated in *Nr3c1*$^{fl/fl}$*Cd4*-cre$^{+}$ T cells, whereas differentiation of IL-4– and IL-13–producing cells was reduced (Figures S7C and S7D). The transcription factor E4BP4 is induced by glucocorticoids (So et al., 2009) and

regulates Th2 cytokine production (Kashiwada et al., 2011; Motomura et al., 2011). Consistent with this, expression of E4BP4, but not GATA binding protein 3 (GATA3) was reduced in *Nr3c1*$^{fl/fl}$*Cd4*-cre$^{+}$ T cells cultured under Th2-inducing conditions (Figure S7E). We next immunized control and *Nr3c1*$^{fl/fl}$*Cd4*-cre$^{+}$ mice with OVA at ZT16. After 7 days, the spleen cells were stimulated with OVA for 3 days. Production of IL-4 and IL-13 was significantly impaired in *Nr3c1*$^{fl/fl}$*Cd4*-cre$^{+}$ mice, and levels of IL-4 and IL-13 mRNAs were also reduced in follicular helper T (Tfh) cells of *Nr3c1*$^{fl/fl}$*Cd4*-cre$^{+}$ mice (Figures S7F and S7G). By contrast, GRE12m mice exhibited no change in Th cell differentiation (Figure S7H). These results suggest that GRs control Th cell differentiation independently of IL-7R expression.

Next, to assess whether the B cell immune response also follows a diurnal rhythm influenced by glucocorticoids, we immunized *Nr3c1*$^{fl/fl}$*Cd4*-cre$^{+}$ mice with OVA at night or daytime. Similar to effector CD8$^{+}$ T cells, this immunization induced Tfh cells, germinal center B cells, and immunoglobulin (Ig) G1$^{+}$ B cells in a diurnal rhythm (high at night and low in the daytime) in control mice, but this diurnal change was impaired in *Nr3c1*$^{fl/fl}$*Cd4*-cre$^{+}$ mice (Figures 6A–C). In addition, production of NP-specific IgG1 and IgG2b was reduced in *Nr3c1*$^{fl/fl}$*Cd4*-cre$^{+}$ mice at night, and the diurnal rhythm was lost (Figure 6D). The diurnal induction of Tfh cells, germinal center B cells, and IgG1$^{+}$ B cells was reduced in GRE12m mice (Figure S7I). These results indicate that GRs control B cell immune responses via Tfh cells in a diurnal fashion, dependent on IL-7R expression.

Peyer's patches are lymphoid tissues in which germinal centers are induced by commensal microbiota even in the absence of immunization (Harada et al., 2012). In Peyer's patches of control mice, the numbers of Tfh cells, germinal center B cells, and IgG1$^{+}$ B cells were unchanged between daytime and night, and their numbers were reduced in *Nr3c1*$^{fl/fl}$*Cd4*-cre$^{+}$ mice (Figures 6E and 6F), whereas those of GRE12m mice exhibited less

distinct reductions (Figure S7J). These results suggest that GRs might have a permissive effect on the T cell–mediated B cell response, independent of IL-7R expression.

**GRs Support Maintenance of Memory CD4$^+$ T Cells by Regulating IL-7R Expression**

Because IL-7R is expressed at higher levels in memory T cells and is critical for their survival (Kondrack et al., 2003; Schluns et al., 2000), we next tested whether glucocorticoids regulate IL-7R expression in memory CD4$^+$ T cells. Because the function of Th2 cells was impaired in *Nr3c1*$^{fl/fl}$*Cd4*-cre$^+$ mice, we generated memory Th2 cells using an adoptive transfer model (Endo et al., 2011). First, we cultured naïve T cells under Th2 conditions for 6 days, and then transferred the effector T cells into B6.CD45.1$^+$ mice. After 4 weeks, we analyzed IL-7R expression in CD45.2$^+$ memory T cells in spleen. Similar to naïve T cells IL-7R expression was reduced in *Nr3c1*$^{fl/fl}$*Cd4*-cre$^+$ and GRE12m memory T cells in comparison with control cells (Figures 7A and 7B). Furthermore, the diurnal change in IL-7R expression was lost in the mutant memory T cells (Figure 7C). The numbers of *Nr3c1*$^{fl/fl}$*Cd4*-cre$^+$ and GRE12m memory T cells were reduced in spleen, lymph nodes, and lungs: *Nr3c1*$^{fl/fl}$*Cd4*-cre$^+$ cells were more severely reduced than GRE12m cells (Figure 7D). As in naïve T cells, Bcl-2 expression was reduced in *Nr3c1*$^{fl/fl}$*Cd4*-cre$^+$ cells, but not in GRE12m cells (Figure 7E). These results indicate that IL-7R induction by GRs is important for maintenance of memory T cells.

**DISCUSSION**

In contrast to the longstanding view that glucocorticoids have strong anti-inflammatory and immunosuppressive effects, this study revealed that glucocorticoids are immunoenhancing. We found that glucocorticoids and GR directly induce IL-7R expression in T cells in diurnal fashion through binding to the IL-7Rα enhancer. The elevated IL-7R induces T cell homing to peripheral lymphoid organs via CXCR4 expression and enhances immune responses of T and

B cells at night in mice. Our use of GRE12m mice was crucial in leading us to this understanding. The diurnal redistribution of T cells by glucocorticoids may facilitate recirculation and long-term survival of a wide range of T cell clones. Because glucocorticoids also induce IL-7R expression in human T cells (Franchimont et al., 2002), it is possible that this immunoenhancing function of glucocorticoids also operates in humans.

Although our findings suggest that glucocorticoids and IL-7 are important for T cell survival, whether or how cell survival contributes to the diurnal redistribution of T cells is not fully understood. Because T cell survival is impaired in *Nr3c1*$^{fl/fl}$*Cd4*-cre$^{+}$ and GRE12m mice, there is a possibility that the impaired survival might have some role in the impaired oscillations in T cell numbers in the mutant mice. However, *Cxcr4*$^{fl/fl}$*Cd4*-cre$^{+}$ mice exhibit substantial impairment of the diurnal redistribution of T cells without any defects in survival, which suggests that the impairment of homing alone does not necessarily lead to decreased cell numbers in blood. Thus, CXCR4 expression seems to play more important role in the diurnal redistribution than cell survival.

Our findings have important implications regarding the circadian changes of the immune system. Blood glucocorticoid levels rise during active phases in daily life, when the risk of injury and infection increase. The resultant T cell accumulation in the spleen would help to combat invading microorganisms. Consistent with this, the immune system is under the control of the diurnal rhythm. Previous studies showed that innate immune cells efficiently respond to bacterial infections at night (Curtis et al., 2014). Circadian CXCL12 expression induces migration of aged neutrophils to bone marrow and their engulfment by tissue-resident macrophages (Casanova-Acebes et al., 2013), and liver X receptor in macrophages regulates circadian expression of phagocytosis-related genes. In addition, the expression of Toll-like receptor (TLR) 9 is high at dusk in macrophages and B cells (Silver et al., 2012). Moreover, the levels of inflammatory cytokines and B7 costimulatory molecules

are higher at night than in daytime in spleen (Silver et al., 2012), suggesting that antigen presentation might be enhanced at night. *In vitro* proliferation of lymph node T cells is more rapid when the cells are isolated at night than during the daytime, largely due to higher signaling molecule ZAP-70 expression, whereas the T cell response is stronger when mice are immunized during the daytime than at night (Fortier et al., 2011). Some of these time points correspond to the glucocorticoid-induced diurnal rhythm of T cell redistribution to the spleen.

The circadian changes of the immune system are controlled by at least three mechanisms. First, adrenergic neural signals regulate the adaptive immune response by diurnal lymphocyte recirculation in lymph nodes (Suzuki et al., 2016). Second, the lymphocyte clock gene *Arntl* controls trafficking through the lymph nodes and immune responses by regulating CCR7 and S1PR1 expression (Druzd et al., 2017). These two pathways are primarily responsible for regulating lymphocyte recirculation through peripheral lymph nodes. Third, glucocorticoids regulate diurnal redistribution of T cells between blood and lymphoid organs and enhance the immune response in spleen. Together, these mechanisms may create the temporal difference in the oscillations of T cell numbers between lymph nodes and spleen. More detailed analysis will help to reveal a more comprehensive view of the diurnal change in lymphocyte distribution in the lymphoid organs.

Glucocorticoids control T cell functions by IL-7R–dependent and –independent mechanisms. We showed that diurnal T cell redistribution via CXCR4 is regulated similarly in *Nr3c1*$^{fl/fl}$*Cd4*-cre$^{+}$ and GRE12m mice, suggesting that this process depends mainly on an IL-7R–dependent mechanism. By contrast, *Nr3c1*$^{fl/fl}$*Cd4*-cre$^{+}$ mice exhibited more severe phenotypes in terms of survival of naïve and memory T cells, as well as the immune response of CD8$^{+}$ T cells, than GRE12m mice. Glucocorticoids probably regulate these immune functions by both IL-7R–dependent and –independent mechanisms. Finally, differentiation of Th subsets and the B cell immune response are impaired in *Nr3c1*$^{fl/fl}$*Cd4*-cre$^{+}$ and GRE12m

mice, suggesting that glucocorticoids regulate these processes mainly via an IL-7R–dependent mechanism. GRs may exert IL-7R–independent functions by activating other target genes, such as *Nfil3*, or by directly interacting with other transcription factors.

GRs control the differentiation and response of Th subsets in multiple mechanisms. Our findings revealed that GRs enhance Th2 cytokine production and the B cell immune response, whereas GRs suppress Th1 differentiation. Glucocorticoids inhibit Th1 differentiation by suppressing transcription factors such as AP-1, NF-κB, and NFAT (Ashwell et al., 2000), and also suppress STAT4 and T box transcription factor 21 (TBX21) signals (Franchimont et al., 2000; Liberman et al., 2007). In addition, our results demonstrate that E4BP4 expression is impaired in *Nr3c1*$^{fl/fl}$*Cd4*-cre$^{+}$ mice. E4BP4 is important for regulation of IL-4 and IL-13 production (Kashiwada et al., 2011), and GRs induce transcription of the *Nfil3* gene by binding to its promoter (So et al., 2009). Therefore, our findings suggest that GRs might enhance IL-4 and IL-13 production by inducing E4BP4. Because *Nfil3* is itself a clock gene, and its expression is higher at night, the GR–E4BP4 axis might be important for the diurnal change in the Th2 immune response. Furthermore, we demonstrate that GRs support the survival of memory Th2 cells via diurnal IL-7R induction. Because the IL-7 signal helps to produce Th2 cytokines (Guo et al., 2015), GRs might enhance the Th2 immune response.

Steroid hormones, including glucocorticoids, mineralocorticoids, androgens, and estrogens, may have a strong influence on the immune system. Not only glucocorticoids, but also androgens and estrogens, are produced from adrenal cortex in diurnal fashion. In this study, we demonstrated that glucocorticoids enhance the responses of T and B cells by inducing IL-7R expression and T cell redistribution to the lymphoid organs. In addition, our study suggests that glucocorticoids prevent Th1 differentiation and augment Th2 differentiation. In addition to glucocorticoids, androgens inhibit Th1 differentiation, whereas

estrogens enhance IFN-γ and IL-10 production (Gilmore et al., 1997; Kissick et al., 2014; Miyaura and Iwata, 2002). Furthermore, these effects might be under the control of the circadian cycle, which might in turn be related to the observation that the symptoms of asthma and rheumatoid arthritis tend to be exacerbated in the morning. Thus, it is likely that many aspects of immunity are under the control of steroid hormones. Future studies should seek to resolve immunological phenomena from the perspective of steroid hormones.

Glucocorticoids may control mucosal immunity by various mechanisms. We revealed that the GR–IL-7R axis induces diurnal T cell homing to Peyer's patches, and that glucocorticoids enhance Tfh cell differentiation and B cell responses in Peyer's patches. These observations suggest a new role for glucocorticoids in mucosal immunity. The mucosal immune system is influenced by circadian oscillations, such as food digestion and the activity of commensal bacteria (Hussain and Pan, 2009). This may in turn trigger TLR activation and inflammatory cytokine production, which, together with T cell accumulation by glucocorticoids, help the mucosal immune system to clear invading bacteria. In addition, intestinal epithelial cells produce glucocorticoids in a circadian fashion (Cima et al., 2004; Hussain and Pan, 2009; Mukherji et al., 2013), suggesting that intestinal glucocorticoids might also enhance mucosal immunity. The roles of glucocorticoids in mucosal immunity should be investigated in future studies.

Because glucocorticoids are stress-responsive hormones, their irregular production during periods of high stress, shift work, and chronic fatigue may cause impairment of the immune functions investigated in this study. On the other hand, clinical administration of synthetic glucocorticoids, which might have stronger affinity for GRs, probably perturbs the diurnal change in endogenous glucocorticoid levels, thereby diminishing the immunoenhancing function of glucocorticoids in the immune system.

**ACKNOWLEDGEMENTS**

We would like to acknowledge Drs. J. Takeda, K. Yusa, and G. Kondoh for providing the KY1.1 ES line and targeting system; and Dr. Batu Erman and members of the K. Ikuta laboratory for discussion. This work was supported by JSPS KAKENHI Grant Numbers 16K15288, 16H05172, and 15H01153 (K.I.), 26460572 (S.T.), and 16K08835 (T.H.); by the Joint Usage/Research Center program of Institute for Frontier Life and Medical Sciences Kyoto University; by the Future Developmental Funding Program of Kyoto University Research Coordination Alliance; and by the Japan Society for the Promotion of Science (JSPS) and TUBITAK Joint Research Project. A.S. was supported by the Platform for Dynamic Approaches to Living System from the Ministry of Education, Culture, Sports, Science and Technology (MEXT) and Japan Agency for Medical Research and Development (AMED). G.C. was an International Research Fellow of the Japan Society for the Promotion of Science.

**AUTHOR CONTRIBUTIONS**

A.S. designed and performed experiments and wrote the paper. G.C., S.T., M.O., S.A., F.O., and T.H. performed some experiments. S.K. and H.M. generated GRE mutant mice. H.Y. and Y.Y. provided LM-OVA and supervised some studies. T.N. provided *Cxcr4*$^{fl/fl}$ and *Cxcl12*-GFP mice. G.S. provided *Nr3c1*$^{fl/fl}$ mice. K.I. conceptualized and supervised studies, designed and performed some experiments, discussed the data, and wrote the paper.

**Declaration of Interests**

The authors have no competing interests to declare.

**REFERENCES**


Abe, A., Tani-ichi, S., Shitara, S., Cui, G., Yamada, H., Miyachi, H., Kitano, S., Hara, T., Abe, R., Yoshikai, Y., and Ikuta, K. (2015). An enhancer of the IL-7 receptor α−chain locus controls IL-7 receptor expression and maintenance of peripheral T cells. J. Immunol. *195*, 3129-3138.

Ara, T., Itoi, M., Kawabata, K., Egawa, T., Tokoyoda, K., Sugiyama, T., Fujii, N., Amagai, T., and Nagasawa, T. (2003). A role of CXC chemokine ligand 12/stromal cell-derived factor-1/pre-B cell growth stimulating factor and its receptor CXCR4 in fetal and adult T cell development in vivo. J. Immunol. *170*, 4649-4655.

Ashwell, J.D., Lu, F.W.M., and Vacchio, M.S. (2000). Glucocorticoids in T cell development and function. Annu. Rev. Immunol. *18*, 309-345.

Casanova-Acebes, M., Pitaval, C., Weiss, L.A., Nombela-Arrieta, C., Chevre, R., A-Gonzalez, N., Kunisaki, Y., Zhang, D.C., van Rooijen, N., Silberstein, L.E., *et al.* (2013). Rhythmic modulation of the hematopoietic niche through neutrophil clearance. Cell *153*, 1025-1035.

Cima, I., Corazza, N., Dick, B., Fuhrer, A., Herren, S., Jakob, S., Ayuni, E., Mueller, C., and Brunner, T. (2004). Intestinal epithelial cells synthesize glucocorticoids and regulate T cell activation. J. Exp. Med. *200*, 1635-1646.

Cui, G.W., Hara, T., Simmons, S., Wagatsuma, K., Abe, A., Miyachi, H., Kitano, S., Ishii, M., Tani-ichi, S., and Ikuta, K. (2014). Characterization of the IL-15 niche in primary and secondary lymphoid organs in vivo. Proc. Natl. Acad. Sci. USA. *111*, 1915-1920.

Curtis, A.M., Bellet, M.M., Sassone-Corsi, P., and O'Neill, L.A.J. (2014). Circadian clock proteins and immunity. Immunity *40*, 178-186.

Dimitrov, S., Benedict, C., Heutling, D., Westermann, J., Born, J., and Lange, T. (2009).

Cortisol and epinephrine control opposing circadian rhythms in T cell subsets. Blood *113*, 5134-5143.

Druzd, D., Matveeva, O., Ince, L., Harrison, U., He, W.Y., Schmal, C., Herzel, H., Tsang, A.H., Kawakami, N., Leliavski, A., *et al.* (2017). Lymphocyte circadian clocks control lymph node trafficking and adaptive immune responses. Immunity *46*, 120-132.

Elenkov, I.J. (2004). Glucocorticoids and the Th1/Th2 balance. Ann. N. Y. Acad. Sci. *1024*, 138-146.

Endo, Y., Iwamura, C., Kuwahara, M., Suzuki, A., Sugaya, K., Tumes, D.J., Tokoyoda, K., Hosokawa, H., Yamashita, M., and Nakayama, T. (2011). Eomesodermin controls interleukin-5 production in memory T helper 2 cells through inhibition of activity of the transcription factor GATA3. Immunity *35*, 733-745.

Fortier, E.E., Rooney, J., Dardente, H., Hardy, M.P., Labrecque, N., and Cermakian, N. (2011). Circadian variation of the response of T cells to antigen. J. Immunol. *187*, 6291-6300.

Franchimont, D., Galon, J., Gadina, M., Visconti, R., Zhou, Y.J., Aringer, M., Frucht, D.M., Chrousos, G.P., and O'Shea, J.J. (2000). Inhibition of Th1 immune response by glucocorticoids, dexamethasone selectively inhibits IL-12-induced Stat4 phosphorylation in T lymphocytes. J. Immunol. *164*, 1768-1774.

Franchimont, D., Galon, J., Vacchio, M.S., Fan, S., Visconti, R., Frucht, D.M., Geenen, V., Chrousos, G.P., Ashwell, J.D., and O'Shea, J.J. (2002). Positive effects of glucocorticoids on T cell function by up-regulation of IL-7 receptor $\alpha$. J. Immunol. *168*, 2212-2218.

Gibbs, J., Ince, L., Matthews, L., Mei, J.J., Bell, T., Yang, N., Saer, B., Begley, N., Poolman, T., Pariollaud, M., *et al.* (2014). An epithelial circadian clock controls pulmonary inflammation and glucocorticoid action. Nat. Med. *20*, 919-926.

Gilmore, W., Weiner, L.P., and Correale, J. (1997). Effect of estradiol on cytokine secretion by

proteolipid protein-specific T cell clones isolated from multiple sclerosis patients and normal control subjects. J. Immunol. *158*, 446-451.

Guo, L.Y., Huang, Y.F., Chen, X., Hu-Li, J., Urban, J.F., and Paul, W.E. (2015). Innate immunological function of $T_H2$ cells in vivo. Nat. Immunol. *16*, 1051-1059.

Hara, T., Shitara, S., Imai, K., Miyachi, H., Kitano, S., Yao, H., Tani-ichi, S., and Ikuta, K. (2012). Identification of IL-7-producing cells in primary and secondary lymphoid organs using IL-7-GFP knock-in mice. J. Immunol. *189*, 1577-1584.

Harada, Y., Tanaka, S., Motomura, Y., Ohno, S., Yanagi, Y., Inoue, H., and Kubo, M. (2012). The 3' enhancer CNS2 is a critical regulator of interleukin-4-mediated humoral immunity in follicular helper T cells. Immunity *36*, 188-200.

Hata, K., Yanase, N., Sudo, K., Kiyonari, H., Mukumoto, Y., Mizuguchi, J., and Yokosuka, T. (2016). Differential regulation of T-cell dependent and T-cell independent antibody responses through arginine methyltransferase PRMT1 in vivo. FEBS Lett. *590*, 1200-1210.

Haus, E., and Smolensky, M.H. (1999). Biologic rhythms in the immune system. Chronobiol. Int. *16*, 581-622.

Hussain, M.M., and Pan, X.Y. (2009). Clock genes, intestinal transport and plasma lipid homeostasis. Trends. Endocrinol. Metab. *20*, 177-185.

Jourdan, P., Vendrell, J.P., Huguet, M.F., Segondy, M., Bousquet, J., Pene, J., and Yssel, H. (2000). Cytokines and cell surface molecules independently induce CXCR4 expression on $CD4^+$ $CCR7^+$ human memory T cells. J. Immunol. *165*, 716-724.

Kanegae, Y., Lee, G., Sato, Y., Tanaka, M., Nakai, M., Sakaki, T., Sugano, S., and Saito, I. (1995). Efficient gene activation in mammalian cells by using recombinant adenovirus expressing site-specific Cre recombinase. Nucleic Acids Res. *23*, 3816-3821.

Kashiwada, M., Cassel, S.L., Colgan, J.D., and Rothman, P.B. (2011). NFIL3/E4BP4 controls type 2 T helper cell cytokine expression. EMBO. J. *30*, 2071-2082.

Kissick, H.T., Sanda, M.G., Dunn, L.K., Pellegrini, K.L., On, S.T., Noel, J.K., and Arredouani, M.S. (2014). Androgens alter T-cell immunity by inhibiting T-helper 1 differentiation. Proc. Natl. Acad. Sci. USA. *111*, 9887-9892.

Kondrack, R.M., Harbertson, J., Tan, J.T., McBreen, M.E., Surh, C.D., and Bradley, L.M. (2003). Interleukin 7 regulates the survival and generation of memory CD4 cells. J. Exp. Med. *198*, 1797-1806.

Lee, H.C., Shibata, H., Ogawa, S., Maki, K., and Ikuta, K. (2005). Transcriptional regulation of the mouse IL-7 receptor α promoter by glucocorticoid receptor. J. Immunol. *174*, 7800-7806.

Lee, P.P., Fitzpatrick, D.R., Beard, C., Jessup, H.K., Lehar, S., Makar, K.W., Perez-Melgosa, M., Sweetser, M.T., Schlissel, M.S., Nguyen, S., *et al.* (2001). A critical role for Dnmt1 and DNA methylation in T cell development, function, and survival. Immunity *15*, 763-774.

Liberman, A.C., Refojo, D., Druker, J., Toscano, M., Rein, T., Holsboer, F., and Arzt, E. (2007). The activated glucocorticoid receptor inhibits the transcription factor T-bet by direct protein-protein interaction. FASEB J. *21*, 1177-1188.

Mazzucchelli, R., and Durum, S.K. (2007). Interleukin-7 receptor expression: intelligent design. Nat. Rev. Immunol. *7*, 144-154.

Miyaura, H., and Iwata, M. (2002). Direct and indirect inhibition of Th1 development by progesterone and glucocorticoids. J. Immunol. *168*, 1087-1094.

Motomura, Y., Kitamura, H., Hijikata, A., Matsunaga, Y., Matsumoto, K., Inoue, H., Atarashi, K., Hori, S., Watarai, H., Zhu, J.F., *et al.* (2011). The transcription factor E4BP4 regulates the production of IL-10 and IL-13 in $CD4^+$ T cells. Nat. Immunol. *12*, 450-U111.

Mukherji, A., Kobiita, A., Ye, T., and Chambon, P. (2013). Homeostasis in intestinal epithelium is orchestrated by the circadian clock and microbiota cues transduced by TLRs. Cell *153*, 812-827.

Pope, C., Kim, S.K., Marzo, A., Masopust, D., Williams, K., Jiang, J., Shen, H., and Lefrancois, L. (2001). Organ-specific regulation of the CD8 T cell response to *Listeria monocytogenes* infection. J. Immunol. *166*, 5840-5840.

Purton, J.F., Boyd, R.L., Cole, T.J., and Godfrey, D.I. (2000). Intrathymic T cell development and selection proceeds normally in the absence of glucocorticoid receptor signaling. Immunity *13*, 179-186.

Schluns, K.S., Kieper, W.C., Jameson, S.C., and Lefrancois, L. (2000). Interleukin-7 mediates the homeostasis of naive and memory CD8 T cells in vivo. Nat. Immunol. *1*, 426-432.

Screpanti, I., Morrone, S., Meco, D., Santoni, A., Gulino, A., Paolini, R., Crisanti, A., Mathieson, B.J., and Frati, L. (1989). Steroid sensitivity of thymocyte subpopulations during intrathymic differentiation effects of 17β-estradiol and dexamethazone on subsets expressing T cell antigen receptor or IL-2 receptor. J. Immunol. *142*, 3378-3383.

Silver, A.C., Arjona, A., Walker, W.E., and Fikrig, E. (2012). The circadian clock controls Toll-like receptor 9-mediated innate and adaptive immunity. Immunity *36*, 251-261.

So, A.Y.L., Bernal, T.U., Pillsbury, M.L., Yamamoto, K.R., and Feldman, B.J. (2009). Glucocorticoid regulation of the circadian clock modulates glucose homeostasis. Proc. Natl. Acad. Sci. USA. *106*, 17582-17587.

Suzuki, K., Hayano, Y., Nakai, A., Furuta, F., and Noda, M. (2016). Adrenergic control of the adaptive immune response by diurnal lymphocyte recirculation through lymph nodes. J. Exp. Med. *213*, 2567-2574.

Tani-ichi, S., Shimba, A., Wagatsuma, K., Miyachi, H., Kitano, S., Imai, K., Hara, T., and

Ikuta, K. (2013). Interleukin-7 receptor controls development and maturation of late stages of thymocyte subpopulations. Proc. Natl. Acad. Sci. USA. *110*, 612-617.

Tokoyoda, K., Egawa, T., Sugiyama, T., Choi, B.I., and Nagasawa, T. (2004). Cellular niches controlling B lymphocyte behavior within bone marrow during development. Immunity *20*, 707-718.

Tronche, F., Kellendonk, C., Kretz, O., Gass, P., Anlag, K., Orban, P.C., Bock, R., Klein, R., and Schutz, G. (1999). Disruption of the glucocorticoid receptor gene in the nervous system results in reduced anxiety. Nat. Genet. *23*, 99-103.

Yajima, T., Nishimura, H., Sad, S., Shen, H., Kuwano, H., and Yoshikai, Y. (2005). A novel role of IL-15 in early activation of memory $CD8^+$ CTL after reinfection. J. Immunol. *174*, 3590-3597.

**Figure Legends**

**Figure 1. GRs control IL-7R expression and distribution of T cells in a diurnal fashion.**

(**A**) Flow cytometry of IL-7R expression on $CD4^+$ T ($CD3^+CD4^+CD25^-NK1.1^-$), $CD8^+$ T ($CD3^+8^+$), and Treg ($CD3^+4^+25^+$) cells in spleen of *Nr3c1*$^{fl/fl}$ (control, Ctrl) and *Nr3c1*$^{fl/fl}$*Cd4*-cre$^+$ (GRcKO) mice at zeitgeber time (ZT) 16. (**B**) Flow cytometry of IL-7R expression on $CD4^+$ T cells in spleen at ZT4 and ZT16. (**C**) IL-7R expression on splenic $CD4^+$ and CD8 $T^+$ cells was analyzed by flow cytometry. Mean fluorescence intensity (MFI) is shown over the course of the day ($n$ = 3–4 per time point). (**D**) *Il7r* mRNA in splenic $CD4^+$ and $CD8^+$ T cells was analyzed by qPCR over the course of the day ($n$ = 3–6). (**E**–**H**) Numbers of $CD4^+$ T, $CD8^+$ T, and Treg cells in peripheral blood (E, $n$ = 3–7), lymph nodes (axillary, inguinal, and mesenteric, F, $n$ = 3–5), spleen (G, $n$ = 3–9), and Peyer's patches (H, $n$ = 3–4) of *Nr3c1*$^{fl/fl}$ (control) and *Nr3c1*$^{fl/fl}$*Cd4*-cre$^+$ (GRcKO) mice over the course of the day. ZT0/24 is double-plotted to facilitate viewing (C and E–H). All data are pooled from two to five independent experiments. Data are means ± SEM. One-way and two-way ANOVA (C–H). *$p < 0.05$, **$p < 0.01$, ***$p < 0.001$, n.s. not significant. See also Figure S1.

**Figure 2. IL-7R induction by GRs regulates the diurnal change in T cell distribution.**

(**A**) Flow cytometry of IL-7R expression on $CD4^+$ T, $CD8^+$ T, and Treg cells in spleen of wild-type (WT) and *Il7r*$^{CNS1.GRE12m/12m}$ (GRE12m, GR12) mice at ZT16. (**B**) IL-7R expression on splenic $CD4^+$ and $CD8^+$ T cells was analyzed by flow cytometry. Mean fluorescence intensity (MFI) is shown over the course of the day ($n$ = 3–4 per time point). (**C**) *Il-7r* mRNA in splenic $CD4^+$ and $CD8^+$ T cells was analyzed by qPCR over the course of the day ($n$ = 3–4). (**D**) GR binding to the CNS-1 region in $CD4^+$ T cells was analyzed by ChIP assay ($n$ = 3). (**E**–**H**) Numbers of $CD4^+$ T, $CD8^+$ T, and Treg cells in peripheral blood (E, $n$ = 3–6), lymph

nodes (axillary, inguinal, and mesenteric, F, $n$ = 3–5), spleen (G, $n$ = 3–8), and Peyer's patches (H, $n$ = 3–6) of wild-type (WT) and GRE12m (GR12) mice over the course of the day. ZT0/24 is double-plotted to facilitate viewing (B and E–H). All data are pooled from two to five independent experiments. Data are means ± SEM. One-way and two-way ANOVA (B, C, and E–H); Student's $t$-test (D). *$p < 0.05$, **$p < 0.01$, ***$p < 0.001$, n.s. not significant. See also Figures S2–S4.

**Figure 3. IL-7R induction by GRs controls the diurnal change in T cell distribution by regulating CXCR4 expression.**

(**A** and **B**) Flow cytometry of CXCR4 expression on splenic CD4$^+$ T cells of *Nr3c1*$^{fl/fl}$ (control, Ctrl) and *Nr3c1*$^{fl/fl}$*Cd4*-cre$^+$ (GRcKO) mice (A) and wild-type (WT) and *Il7r*$^{CNS1.GRE12m/12m}$ (GRE12m, GR12) mice (B) at ZT4 and ZT16. (**C** and **D**) Mean fluorescence intensity (MFI) in control and *Nr3c1*$^{fl/fl}$*Cd4*-cre$^+$ mice (C) or wild-type (WT) and GRE12m (GR12) mice (D) at ZT4 and ZT16 ($n$ = 3–4 per time point). (**E** and **F**) qPCR analysis of *Cxcr4* mRNA in CD4$^+$ and CD8$^+$ T cells in spleens of *Nr3c1*$^{fl/fl}$ (control, Ctrl) and *Nr3c1*$^{fl/fl}$*Cd4*-cre$^+$ (GRcKO) mice (E) or wild-type (WT) and GRE12m (GR12) mice (F) over the course of the day ($n$ = 3–4). (**G** and **H**) Chemotaxis of naïve CD4$^+$ T cells toward CXCL12 was assessed by Transwell assay. T cells were isolated from lymph nodes of *Nr3c1*$^{fl/fl}$ (Ctrl) and *Nr3c1*$^{fl/fl}$*Cd4*-cre$^+$ (GRcKO) mice (G) or wild-type (WT) and GRE12m (GR12) mice (H) at ZT4 and ZT16 ($n$ = 3). (**I** and **J**) *In vivo* homing assay. Mice were sacrificed at ZT4 or ZT16, and naïve CD4$^+$ T cells from lymph nodes of control CD45.1$^+$ (C57BL/6) and CD45.2$^+$ (*Nr3c1*$^{fl/fl}$*Cd4*-cre$^+$ [GRcKO] or GRE12m [GR12]) mice were mixed at a 1:1 ratio, labeled with CFSE, and transferred into CD45.2$^+$ C57BL/6 mice at ZT6 (Daytime) or ZT18 (Night), respectively. CFSE$^+$ donor cells were analyzed after 1 hour in spleen, lymph nodes, and peripheral blood. Percentage of donor cells from CD45.1$^+$ control mice and CD45.2$^+$ mutant (*Nr3c1*$^{fl/fl}$*Cd4*-cre$^+$

[I] or GRE12m [J]) mice in total CFSE$^+$ donor cells of the indicated tissues normalized by pre-transfer percentage of donor cells are shown ($n$ = 3–4). (**K**–**M**) Numbers of CD4$^+$ T, CD8$^+$ T, and Treg cells in peripheral blood (K, $n$ = 3–5), lymph nodes (axillary, inguinal, and mesenteric, L, $n$ = 3–5), and spleen (M, $n$ = 3–5) of *Cxcr4*$^{fl/fl}$ (control, Ctrl) and *Cxcr4*$^{fl/fl}$*Cd4*-cre$^+$ (CXCR4cKO) mice over the course of the day. All data are pooled from two to three independent experiments. Data are means ± SEM. One-way and two-way ANOVA (E, F, and K–M). Student's *t*-test (C, D, and G–J). *$p$ < 0.05, **$p$ < 0.01, ***$p$ < 0.001, n.s. not significant. See also Figure S5.

**Figure 4. Upregulation of CXCR4 expression by GRs induces T cell migration to CXCL12-producing cells.**

(**A** and **B**) Immunohistochemistry of spleen from *Cxcl12*-GFP mice. Wild-type T cells were isolated from lymph nodes at ZT16, labeled with CMTMR, and transferred at ZT18. After 1 hour, spleen was isolated and analyzed. White arrowheads indicate *Cxcl12*-GFP$^+$ CD31$^+$ vessels surrounded by CMTMR$^+$ donor cells in the T cell zone (A) and B cell zone (B). Scale bars, 100 μm. **(C** and **D)** Immunohistochemistry of spleen from *Il7*–GFP mice. Wild-type T cells were isolated from lymph nodes at ZT16, labeled with CMTMR, and transferred at ZT18. After 1 hour, spleen was isolated and analyzed. White arrowheads indicate CD31$^+$ vessels surrounded by IL-7$^+$ stromal cells and CMTMR$^+$ donor cells in the T cell zone (C) and B cell zone (D). Scale bars, 100 μm. **(E)** Immunohistochemistry of spleen from *Cxcl12*-GFP mice. T cells from lymph nodes of *Nr3c1*$^{fl/fl}$ (control) and *Nr3c1*$^{fl/fl}$*Cd4*-cre$^+$ (GRcKO) mice were labeled with CellTracker Deep Red (blue) and CMTMR (red), respectively, mixed at a 1:1 ratio, and transferred into *Cxcl12*-GFP mice. After 1 hour, spleen was isolated and analyzed. White arrowheads indicate *Cxcl12*-GFP$^+$ cells surrounded by CMTMR$^+$ and CellTracker Deep Red$^+$ donor cells. Scale bars, 100 μm. (**F**) Percentage of *Nr3c1*$^{fl/fl}$ (control) and

*Nr3c1*$^{fl/fl}$*Cd4*-cre$^{+}$ (GRcKO) T cells among total labeled cells present within 50 μm of *Cxcl12*-GFP$^{+}$ cells in the B cell zone, T cell zone, and red pulp in (E) ($n$ = 4). All data are pooled from two independent experiments. Data are means ± SEM. Student's $t$-test, ***$p$ < 0.001. See also Figure S6.

**Figure 5. GRs regulate diurnal change in clonal expansion and immune response of T cells.**

(**A**) Naïve CD4$^{+}$ and CD8$^{+}$ T cells were isolated from lymph nodes at ZT16 and stimulated with anti-CD3 antibody, anti-CD28 antibody, and human IL-2 for 96 hours. Proliferation of naïve CD4$^{+}$ and CD8$^{+}$ T cells from *Nr3c1*$^{fl/fl}$ (control) and *Nr3c1*$^{fl/fl}$*Cd4*-cre$^{+}$ (GRcKO) mice was assessed by CFSE dilution assay. Divided cells were gated (upper panels) and compared (lower bar graphs, $n$ = 3). (**B**) CD4$^{+}$ and CD8$^{+}$ T cells were isolated from lymph nodes at ZT16 and stimulated with anti-CD3 and anti-CD28 antibodies for 48 hours. IL-2R expression was analyzed by flow cytometry (left panels), and MFIs were compared (right bar graphs, $n$ = 3-4). (**C**) CD4$^{+}$ and CD8$^{+}$ T cells were isolated from lymph nodes at ZT16 and cultured with anti-CD3 and anti-CD28 antibodies for 48 hours, and then stimulated with human IL-2 for 90 minutes. Intracellular staining of phosphorylated STAT5 was analyzed by flow cytometry (left panels), and MFIs were compared (right bar graph, $n$ = 3). (**D**–**G**) *Nr3c1*$^{fl/fl}$ (control, Ctrl) and *Nr3c1*$^{fl/fl}$*Cd4*-cre$^{+}$ (GRcKO) mice (D and E) or wild-type (WT) and *Il7r*$^{CNS1.GRE12m/12m}$ (GR12m, GR12) mice (F and G) were infected with *Listeria monocytogenes* expressing ovalbumin (rLM-OVA) at ZT4 and ZT16. After 7 days (168 hours), OVA$_{257-264}$/K$^{b}$ MHC tetramer$^{+}$ cells were analyzed by flow cytometry. Proportion of MHC tetramer$^{+}$ cells in CD8$^{+}$ T cells (D and F, and left bar graphs in E and G) and numbers of MHC tetramer$^{+}$ cells (right bar graphs in E and G) in *Nr3c1*$^{fl/fl}$ and *Nr3c1*$^{fl/fl}$*Cd4*-cre$^{+}$ mice ($n$ = 4–5) or wild-type and GR12m mice ($n$ = 5–6) are shown. All data are pooled from two to three independent

experiments. Data are means ± SEM. Student's *t*-test, *$p < 0.05$, **$p < 0.01$, n.s. not significant. See also Figure S7.

**Figure 6. GRs control differentiation of Th subsets and humoral immune responses.**

(**A**–**C**) *Nr3c1*$^{fl/fl}$ (control, Ctrl) and *Nr3c1*$^{fl/fl}$*Cd4*-cre$^{+}$ (GRcKO) mice were immunized with OVA at ZT4 or ZT16. After 12 days (288 hours), PD-1$^{+}$CXCR5$^{+}$ Tfh cells, GL7$^{+}$CD95$^{+}$ germinal center B cells, and IgG1$^{+}$ B cells were analyzed at ZT4 or ZT16, respectively, by flow cytometry. Flow cytometric profiles (upper panels) and the proportions and numbers (lower bar graphs) of Tfh cells (A), GL7$^{+}$ germinal center B cells (B), and IgG1$^{+}$ B cells (C) ($n$ = 4–8). (**D**) *Nr3c1*$^{fl/fl}$ (control, Ctrl) and *Nr3c1*$^{fl/fl}$*Cd4*-cre$^{+}$ (GRcKO) mice were immunized with NP-OVA at ZT4 and ZT16. After 20 days, mouse serum was recovered at ZT4 and ZT16, respectively, and the levels of NP-specific immunoglobulins were measured by ELISA ($n$ = 5–7). (**E**) Proportion of CXCR5$^{+}$PD-1$^{+}$ Tfh cells, GL7$^{+}$CD95$^{+}$ germinal center B cells, and IgG1$^{+}$ B cells in Peyer's patches of *Nr3c1*$^{fl/fl}$ (control, Ctrl) and *Nr3c1*$^{fl/fl}$*Cd4*-cre$^{+}$ (GRcKO) mice analyzed at ZT16 by flow cytometry. (**F**) Cell numbers of the cell populations at ZT4 and ZT16 in (E) ($n$ = 4–5). All data are pooled from two to three independent experiments. Data are means ± SEM. Student's *t*-test, *$p < 0.05$, **$p < 0.01$, ***$p < 0.001$. See also Figure S7.

**Figure 7. GRs support maintenance of memory CD4$^{+}$ T cells by inducing IL-7R expression.**

(**A**) Th2 cells were induced from naïve CD4$^{+}$ T cells isolated from lymph nodes of *Nr3c1*$^{fl/fl}$ (control, Ctrl), *Nr3c1*$^{fl/fl}$*Cd4*-cre$^{+}$ (GRcKO), and *Il7r*$^{CNS1.GRE12m/12m}$ (GRE12m, GR12) mice. Flow cytometry was performed to detect CD4$^{+}$ T cells in spleen of CD45.1$^{+}$ mice at 4 weeks after transfer of CD45.2$^{+}$ Th2 cells. (**B**) Flow cytometry of IL-7R expression on

$CD4^+CD45.2^+$ memory Th2 cells in spleen at ZT16. (**C**) qPCR analysis of *Il-7r* mRNA, in memory CD4 T cells in spleen at ZT4 and ZT16 ($n$ = 3–4). Student's $t$-test. (**D**) Numbers of memory $CD4^+$ T cells in spleen ($n$ = 5), lymph nodes (axillary, inguinal, and mesenteric, LN, $n$ = 4), and lungs ($n$ = 4). One-way ANOVA with Tukey's multiple-comparisons test. (**E**) Flow cytometry of Bcl-2 expression in memory $CD4^+$ T cells. All data are pooled from two to three independent experiments. Data are means ± SEM. *$p < 0.05$, **$p < 0.01$, ***$p < 0.001$.

## STAR METHODS

## CONTACT FOR REAGENT AND RESOURCE SHARING

Further information and requests for resources and reagents should be directed to the Lead Contact, Dr. Koichi Ikuta (ikuta.koichi.6c@kyoto-u.ac.jp).

## EXPERIMENTAL MODEL AND SUBJECT DETAILS

### Mice

B6.SJL-*Ptprc*$^{a}$ *Pepc*$^{b}$/BoyJ (B6.CD45.1 congenic), B6.Cg-Tg(Cd4-cre)1Cwi (*Cd4*-cre) (Lee et al., 2001), B6.129-*Nr3c1*$^{tm2Gsc}$ (*Nr3c1*$^{fl/fl}$) (Tronche et al., 1999), B6.129-*Cxcr4*$^{tm2Tng}$ (*Cxcr4*$^{fl/fl}$) (Tokoyoda et al., 2004), B6.129-*Il7r*$^{tm2Iku}$(*Il7r*$^{fl/fl}$) (Tani-ichi et al., 2013), B6.129-*Cxcl12*$^{tm2Tng}$ (*Cxcl12*-GFP) (Ara et al., 2003), and B6.129-*Il7*$^{tm1.1Iku}$ (*Il7*–GFP) (Hara et al., 2012) mice were used. All mice were maintained under specific pathogen–free conditions in the Experimental Research Center for Infectious Diseases in the Institute for Frontier Life and Medical Sciences, Kyoto University. Experiments were performed on 6–12-week-old male and female mice. For infection or immunization assays, experiments were performed on 8–14-week-old male and female mice. Each pair of control and mutant mice of the same sex from the same litter was analyzed simultaneously, and the data were pooled from multiple pairs of mixed sex derived from multiple litters, except for the experiments in Figures 2D, 3I, 3J, S4C, and S4D, where mice from the different litters were analyzed simultaneously. All procedures were carried out under Sevoflurane anesthesia to minimize animal suffering. Mice were housed in group under controlled conditions of humidity, temperature, and light (12-hr light/12-hr dark cycles). Food and water were

available *ad libitum*. All mouse protocols were approved by the Animal Experimentation Committee of the Institute for Frontier Life and Medical Sciences, Kyoto University.

**Generation of GRE Mutant Mice**

To construct a targeting vector, the following DNA fragments were assembled in vector pBluescript KS (+): a diphtheria toxin A cassette, a 1,822-bp fragment of the 5' CNS1 element of the IL-7Rα locus, a neomycin resistance gene cassette flanked by *lox*P sequences, and an 8,521-bp fragment containing a mutated CNS1 element and 3' CNS1 region. *In vitro* mutagenesis of the CNS1 element was carried out using the QuikChange site-directed mutagenesis kit (Agilent Technologies). GRE1 and GRE2 mutations were as follows, with mutated nucleotides underlined: GRE1 wild-type, 5'-CTTTGTTCTTTTACATCTTCA-3'; GRE1m, 5'-CTTCACTGCTTTGAGTGCTCA-3'; GRE2 wild-type, 5'-TAGCACATGCTGTACC-3'; and GRE2m, 5'-TAGCGAGTGCTGTACC-3'. The linearized vector was introduced into KY1.1 ES cells (C57BL/6 × 129S6/SvEvTac F1 background) by electroporation, and homologous recombinants were screened by PCR. Targeted ES clones were confirmed by Southern blot analysis with 5' and 3' probes (Figures S2A–S2C). The neomycin resistance gene cassette was removed from the recombinant allele by infecting targeted ES clones *in vitro* with adenovirus expressing Cre recombinase, AdV-Cre (a kind gift of Dr. Izumu Saito of the Institute of Medical Science, The University of Tokyo). The resultant ES clones contained one copy of the *lox*P site 5' of the mutated CNS1 element. ES clones were injected into ICR 8-cell embryos. Chimeric mice were bred with C57BL/6 mice, and GRE mutant mice were backcrossed onto the C57BL/6 background for nine generations.

**Bacterial Infection**

Recombinant *Listeria monocytogenes* expressing OVA (rLM-OVA) were described previously (Abe et al., 2015; Pope et al., 2001; Yajima et al., 2005). Mice were injected intravenously with $2.5 \times 10^4$ CFU rLM-OVA at ZT4 or ZT16. After 7 days (168 hours), spleen cells were stained with antibodies. Flow cytometry was performed after the cells were fixed in 0.1% paraformaldehyde in PBS for 20 minutes at 4°C.

## METHOD DETAILS

### Cell Preparation

After perfusion, lungs were minced with scissors and incubated at 37°C for 1 hour in RPMI-1640 medium containing 10% FBS, 1 mg/ml collagenase D, and 50 μg/ml DNase I. Digested lung fragments were passed through a 40-μm strainer. Leukocytes were separated by centrifugation through 30% Percoll. After lysis of red blood cells, cells were analyzed by flow cytometry.

### Antibodies and Flow Cytometry

Cells were prepared from the indicated organs and stained with antibodies for 20 minutes at 4°C in PBS containing 0.05% $NaN_3$ and 0.1% bovine serum albumin (BSA). Fluorescent dye- or biotin-conjugated antibodies against the following proteins were purchased from BD Bioscience, eBioscience, BioLegend, Invitrogen, or TONBO Biosciences: CD3ε (145-2C11), TCRβ (H57-597), CD4 (RM4.5), CD8α (53-6.7), CD11a (M17/4), CD25 (7D4), CD44 (IM7), NK1.1 (PK136), CD69 (H1.2F3), PD-1 (29F.1A12), CXCR4 (L276F12), CXCR5 (L138D7), CCR7 (4B12), CD62L (MEL-14), CD95 (Jo2), GL7 antigen (GL7) CD45R/B220 (RA3-6B2), CD19 (6D5), IgG1 (RMG1-1), IFN-γ (XMG1.2), IL-2 (JES6-5H4), IL-4 (11B11), IL-13 (eBio 13A), E4BP4 (S2M-E19), GATA3 (16E10A23), CD45.2 (104), CD122 (TM-beta1),

CD127 (A7R34), phosophorylated-STAT5 (47), and Bcl-2 (A19-3). H-2K$^{b}$ OVA G4 tetramer-SIIGFEKL-PE was purchased from Medical and Biological Laboratories. Biotinylated monoclonal antibodies were detected with PE- or Brilliant Violet 421–conjugated streptavidin (eBioscience). Viable cells were analyzed on a FACSCanto II flow cytometer (BD Biosciences) using the FlowJo software. In the figures, values in quadrants, gated areas, and interval gates indicate percentages in each population.

For intracellular staining of Bcl-2, GATA3, and E4BP4, T cells were stained for surface antigens, fixed, permeabilized, and stained with relevant antibodies using the Foxp3 Staining Buffer Set (eBioscience). For intracellular staining of cytokine production, cultured CD4$^{+}$ T cells were fixed, permeabilized, and stained with the relevant antibodies using IC Fixation Buffer (eBioscience). For intracellular staining for phosophorylated-STAT5, the cells were fixed, permeabilized in ice-cold methanol, and stained with anti-phosphorylated STAT5 antibody using the Foxp3 Staining Buffer Set.

**Cell Isolation**

Naïve CD4$^{+}$ and CD8 T$^{+}$ cells were purified from lymph nodes using EasySep Naïve CD4 and CD8 T-Cell Enrichment kits (STEMCELL Technologies). For qPCR analysis, CD4$^{+}$ T (CD3$^{+}$CD4$^{+}$CD25$^{-}$NK1.1$^{-}$), CD8$^{+}$ T (CD3$^{+}$CD8$^{+}$), Treg (CD3$^{+}$CD4$^{+}$CD25$^{+}$), and Th2 memory (CD4$^{+}$CD45.2$^{+}$) cells were sorted from thymus and spleen with a FACSAria II cell sorter (BD Biosciences). For immunohistochemistry, T cells were purified using the Pan T Cell Isolation Kit (Miltenyi Biotech). Density of white blood cells in peripheral blood was measured on a Celltacα MEK6450 fully automatic blood cell counter (Nihon Kohden Corp.)

**Cell Culture**

Purified T cells were cultured in RPMI 1640 medium containing 10% fetal bovine serum

(FBS), 50 μM 2-mercaptethanol, and 10 mM HEPES (pH 7.4). To check IL-7Rα expression, cells were cultured with $10^{-8}$ M dexamethasone (Sigma) for 12 hours. For CFSE dilution assay, naïve $CD4^+$ and $CD8^+$ T cells were labeled with 2 μM CFSE (Dojindo Laboratories) in PBS at 37°C for 10 minutes. Cells were cultured with 4 μg/ml plate-bound anti-CD3 antibody, 4 μg/ml soluble anti-CD28 antibody (PV-1, a kind gift from Dr. R. Abe at Tokyo University of Science), and 20 ng/ml human IL-2 (BioLegend). After 96 hours, cells were analyzed by flow cytometry. For *in vitro* survival assays, naïve $CD4^+$ and $CD8^+$ T cells were cultured with 5 ng/ml IL-7 (BioLegend), and the proportions of propidium iodide–negative (i.e., living) cells were measured by flow cytometry at the indicated time points.

**Real-Time PCR**

Total RNA was isolated and reverse-transcribed using random primers. cDNA was analyzed by real-time RT-PCR using SYBR Green PCR Master Mix (QIAGEN) in an ABI7500 real time PCR system (Applied Biosystems). PCR results were normalized against the corresponding levels of *Gapdh* mRNA in cDNA from lymph node cells of wild-type mice. The following primer were used: *Gapdh*, 5'-CCTCGTCCCGTAGACAAAATG-3' and 5'-TCTCCACTTTGCCACTGCAA-3'; *Il7r*, 5'-GGATGGAGACCTAGAAGATG-3' and 5'-GAGTTAGGCATTTCACTCGT-3'; *Cxcr4*, 5'-TGTTGCCATGGAACCGATCA-3' and 5'-TGGTGGGCAGGAAGATCCTA-3'; *Bcl2*, 5'-TCGCTACCGTCGTGACTTC-3' and 5'-AAACAGAGGTCGCATGCTG-3'; *Bclxl*, 5'-GGAGAGCGTTCAGTGATC-3' and 5'-CAATGGTGGCTGAAGAGA-3'; *Il4*, 5'-AGGAGCCATATCCACGGATG-3' and 5'-ACAGACGAGCTCACTCTCTG-3'; *Il13*, 5'-CAGCTCCCTGGTTCTCTCAC-3' and 5'-ACACTCCATACCATGCTGCC-3'.

**Chromatin Immunoprecipitaion Assay (ChIP)**

ChIP was performed as described previously (Lee et al., 2005). Briefly, $5 \times 10^6$ naïve $CD4^+$ T cells were fixed in 1% formaldehyde for 5 minutes at room temperature. Soluble chromatin was immunoprecipitated with 5 μg of anti-GR antibody (BuGR-2, Merck) or mouse IgG (Jackson ImmunoResearch) overnight. Purified ChIP and input DNAs were measured by real-time PCR. PCR primers used for detecting the CNS-1 region were CNS-1/F, 5'-CCATTGCTCACCCACAATCTC-3'; CNS-1/R, 5'-GCTATCACTCCATGGTGAAC-3'.

**Transwell Migration Assay**

Naïve $CD4^+$ T cells were suspended in serum-free medium (RPMI 1640 containing 1% BSA, 10 mM HEPES [pH 7.4]). Migration assay was performed in Transwell chambers with polycarbonate membranes with 5-μm pore diameter (Corning). Medium containing 100 ng/ml CXCL12 (TONBO) was added to the lower chamber, and the membranes were placed on top. T cells ($1 \times 10^5$) were loaded into the upper chamber and cultured for 2 hours at 37°C. Cells in the lower chamber were collected and analyzed by flow cytometry.

**In Vivo Homing Assay**

Mice were sacrificed at ZT4 or ZT16, and purified naïve $CD4^+$ T cells from control $CD45.1^+$ (C57BL/6) and $CD45.2^+$ (*Nr3c1*$^{fl/fl}$*Cd4*-cre$^+$ or *Il7r*$^{CNS1.GRE12m/12m}$) mice were mixed at a 1:1 ratio, labeled with CFSE, and transferred into $CD45.2^+$ C57BL/6 mice ($5 \times 10^6$ total) at ZT6 or ZT18, respectively. The precise pre-transfer percentages of donor cells were determined by analyzing the remaining donor cells by flow cytometry. $CFSE^+$ donor cells were analyzed after 1 hour in spleen, lymph nodes, and peripheral blood. Percentage of donor cells from $CD45.1^+$ control mice and $CD45.2^+$ mutant (*Nr3c1*$^{fl/fl}$*Cd4*-cre$^+$ or *Il7r*$^{CNS1.GRE12m/12m}$) mice in total $CFSE^+$ donor cells of the indicated tissues were normalized by the pre-transfer percentage of donor cells.

**Immunohistochemistry**

Mice were sacrificed at ZT16, and T cells purified from lymph nodes were labeled with CMTMR (Setareh Biotech) or CellTracker Deep Red (Thermo Fisher Scientific) and transferred into *Cxcl12*-GFP and *Il7*-GFP mice at ZT18. After 1 hour, spleen from recepient mice was fixed with 4% paraformaldehyde for 6 hours. Tissue sections were prepared and analyzed as described previously (Cui et al., 2014). After blocking, samples were stained with anti-TCRβ (H57-597), anti-B220 (RA3-6B2), anti-CD31 (MEC13.3), anti-rabbit IgG (Poly4064), anti-GFP rabbit polyclonal antibodies, and streptavidin–Brilliant Violet 421 to detect the T cell zone, B cell zone, and IL-7 signal, and then mounted with PermaFluor mounting medium (Shandon). Confocal imaging was performed on a TSC-SP8 microscope (Leica Microsystems).

**Dexamethasone Administration**

Dexamethasone 21-phosphate disodium salt (200 μg) (Sigma) or PBS was injected intraperitoneally at ZT0. After 4 hours (at ZT4), the mice were sacrificed.

**Caspase Assay**

Naïve $CD4^+$ T cells were purified at ZT4 or ZT16, and cultured in medium for 3 hours without IL-7. Active caspase-3 expression was detected with CaspGLOW Fluorescein Active Caspase-3 Staining Kit (Thermo Fisher Scientific) by flow cytometry.

**Immunization**

Mice were immunized by intraperitoneal injection with 100 μg of OVA (grade V, Sigma Aldrich) emulsified in alum (Thermo Scientific) at ZT16. Splenocytes were isolated after 7

days and stimulated with 100 μg/ml OVA for 72 hours. After stimulation, cytokines in culture supernatant were measured by ELISA (eBioscience). Tfh cells ($TCR\beta^+CD4^+CD44^+CXCR5^+$ $PD\text{-}1^+$) were sorted, and their mRNA was purified. To analyze germinal center B cells, mice were immunized by intraperitoneal injection with 100 μg of OVA emulsified in alum at ZT4 or ZT16. After 12 days, spleen cells were stained with antibodies and analyzed by flow cytometry. For antibody production, mice were immunized by intraperitoneal injection with 100 μg of NP-OVA (LGC Biosearch Technologies) emulsified in alum at ZT16. After 20 days, serum was collected and analyzed by ELISA as described previously (Hata et al., 2016).

**Induction of Th Subsets**

Naïve $CD4^+$ T cells isolated at ZT4 and ZT16 were cultured with 4 μg/ml plate-bound anti-CD3, 4 μg/ml soluble anti-CD28, and 20 ng/ml hIL-2 in the presence of IL-12 (10 ng/ml) and anti-IL-4 antibody (5 ng/ml) for Th1 differentiation, or IL-4 (10 ng/ml) and anti-IFN-γ antibody (5 ng/ml) for Th2 differentiation. After 7 days, the cells were restimulated with PMA (50 ng/ml) and ionomycin (2 μg/ml) for 4 hours in the presence of Brefeldin A. After restimulation, cells were fixed, permeabilized, and stained with the indicated antibodies against cytokines.

**Generation of Memory $CD4^+$ T Cells**

Naïve $CD4^+$ T cells purified from *Nr3c1*$^{fl/fl}$ (Control), *Nr3c1*$^{fl/fl}$*Cd4*-$cre^+$ (GRcKO), or *Il7r*$^{CNS1.GRE12m/12m}$ (GRE12m) mice were cultured under Th2 conditions for 6 days. The effector cells ($2.5 \times 10^7$) were transferred into B6.$CD45.1^+$ mice. After 4 weeks, the recipient mice were sacrificed, and lymphocytes from spleen, lymph nodes, and lungs were analyzed by flow cytometry.

## QUANTIFICATION AND STATISTICAL ANALYSIS

All data are presented as means ± SEM. Comparisons between two samples were performed using the unpaired two-tailed Student's *t*-test. One-way ANOVA analyses followed by Tukey's multiple-comparisons test and two-way ANOVA analyses were used for multiple group comparisons. Statistical analyses were performed using the GraphPad Prism 7 software. $*p < 0.05$, $**p < 0.01$, and $***p < 0.001$.

**Legend to Supplemental Figures**

**Figure S1, related to Figure 1: GRs upregulate IL-7Rα expression in thymic Treg cells.**

(**A**) $CD4^+$ T cells from lymph nodes of *Nr3c1*$^{fl/fl}$ (control) and *Nr3c1*$^{fl/fl}$*Cd4*-cre$^+$ (GRcKO) mice at ZT4 were cultured with or without $10^{-8}$ M dexamethasone (DEX) for 20 hours. IL-7R expression was analyzed by flow cytometry. (**B**) Surface IL-7R expression of thymocytes from *Nr3c1*$^{fl/fl}$ (control) and *Nr3c1*$^{fl/fl}$*Cd4*-cre$^+$ (GRcKO) mice at ZT16. (**C**) qPCR analysis of *Il7r* mRNA in thymocyte subsets at ZT16 ($n$ = 3–4). (**D**) Flow cytometry of thymocyte subsets. (**E**) Cell numbers of thymocyte subsets: DN ($CD4^-8^-$), DP ($CD4^+8^+$), $CD4^+$ SP ($CD4^+8^-25^-NK1.1^-$), and $CD8^+$ SP ($CD4^-8^+$) ($n$ = 18). (**F**) Numbers of Treg ($CD4^+25^+$) and natural killer T (NKT) ($CD3^+NK1.1^+$) cells ($n$ = 18). (**G**) Flow cytometry of thymocyte maturation stages. (**H**) Cell numbers at the indicated stages of thymocyte maturation: stage 1 (S1, $CD69^+TCR\beta^{int}$), stage 2 (S2, $CD69^+TCR\beta^{high}$), and stage 3 (S3, $CD69^-TCR\beta^{high}$) ($n$ = 6). All data are pooled from two-four independent experiments. Data are means ± SEM. Student's $t$-test, $^*p < 0.05$.

**Figure S2, related to Figure 2: Generation of GRE mutant mice.**

(**A**) Schematic illustration of the IL-7Rα locus, targeting vector, and CNS1-targeted alleles. Boxes and the oval indicate exons and CNS1, respectively. Triangles indicate *loxP* sequences. Probes for Southern blot analysis are shown as horizontal bars. N, neomycin resistance gene cassette; E, *Eco*RV; S, *Sph*I. (**B**) Point mutations in GRE1 and GRE2 in GRE mutant mice. X indicates point mutations in GR consensus motifs. (**C**) Southern blot analysis of targeted ES clones. Genomic DNA from two ES clones for each mutant was digested with *Eco*RV and *Sph*I and hybridized with probes A and B, respectively. (**D**) IL-7R expression was analyzed by flow cytometry. CD4 T cells from lymph nodes of wild-type (WT) and *Il7r*$^{CNS1.GRE12m/12m}$ (GRE12m, GR12) at ZT4 mice were cultured with or without $10^{-8}$ M dexamethasone (DEX)

for 20 hours. (**E**) Surface IL-7R expression on $CD4^+$ T, $CD8^+$ T, and Treg cells in spleen of WT, *Il7r*$^{CNS1.GRE1m/1m}$ (GRE1m, GR1), *Il7r*$^{CNS1.GRE2m/2m}$ (GRE2m, GR2), and *Il7r*$^{CNS1.GRE12m/12m}$ (GRE12m, GR12) mice at ZT16. (**F**) qPCR analysis of *Il7r* mRNA expression in splenic $CD4^+$ T and $CD8^+$ T cells of wild-type, GRE1m, GRE2m, and GRE12m mice at ZT16 ($n$ = 4). All data are pooled from two to three independent experiments. Data are means ± SEM. Student's $t$-test, *$p < 0.05$, **$p < 0.01$, ***$p < 0.001$, n.s. not significant.

**Figure S3, related to Figure 2: Phenotypes of GRE mutant and T cell-specific IL-7R–deficient mice.**

(**A**) Surface IL-7R expression in thymocytes of wild-type (WT) and *Il7r*$^{CNS1.GRE12m/12m}$ (GRE12m, GR12) mice at ZT16. (**B**) QPCR analysis of *Il7r* mRNA in thymocyte subsets at ZT16 ($n$ = 3–4). (**C**) Cell numbers of thymocyte subsets: DN ($CD4^-8^-$), DP ($CD4^+8^+$), $CD4^+$ SP ($CD4^+8^-25^-NK1.1^-$), and $CD8^+$ SP ($CD4^-8^+$) cells ($n$ = 6). (**D**) Numbers of Treg ($CD4^+25^+$) and NKT ($CD3^+NK1.1^+$) cells in thymus ($n$ = 6). (**E**–**G**) Numbers of $CD4^+$ T, $CD8^+$ T, and Treg cells at ZT4 and ZT16 in peripheral blood (E), spleen (F), and lymph nodes (axillary, inguinal, and mesenteric, G) of *Il7r*$^{fl/fl}$ (control, Ctrl) and *Il7r*$^{fl/fl}$*Cd4*-cre$^+$ (IL-7RcKO) mice ($n$ = 5–8). All data are pooled from two to four independent experiments. Data are means ± SEM. Student's $t$-test, *$p < 0.05$, **$p < 0.01$, ***$p < 0.001$.

**Figure S4, related to Figure 2: IL-7R induction by GRs support survival of T cells.**

(**A** and **B**) Naïve $CD4^+$ and $CD8^+$ T cells were isolated from lymph nodes of *Nr3c1*$^{fl/fl}$ (control, closed circle) and *Nr3c1*$^{fl/fl}$*Cd4*-cre$^+$ (GRcKO, open circle) mice (A) or wild-type (WT, closed square) and *Il7r*$^{CNS1.GRE12m/12m}$ (GRE12m, open square) mice **(**B) at ZT16, and cultured with IL-7 for 6 days. Live cells were counted by flow cytometry at the indicated time points ($n$ = 3). (**C** and **D**) $CD44^{low}$ $CD4^+$ T cells were purified from lymph nodes of $CD45.1^+$ (C57BL/6) and

CD45.2$^+$ (*Nr3c1*$^{fl/fl}$*Cd4*-cre$^+$, GRcKO [C, $n$ = 3] or GRE12m, GR12 [D, $n$ = 4]) mice at ZT4, mixed at a 1:1 ratio, labeled with CFSE, and transferred into CD45.2$^+$C57BL/6 mice ($5 \times 10^6$ total). CFSE$^+$ donor cells were analyzed after 8 days at ZT4 in spleen, lymph nodes (LN), and peripheral blood. Percentage of CD45.2$^+$ and CD45.2$^-$ populations in CFSE$^+$CD4$^+$ T cells is shown. (**E**) Activated caspase 3 was analyzed by flow cytometry in CD4$^+$ T cells purified from lymph nodes at ZT4 or ZT16 of *Nr3c1*$^{fl/fl}$ (control) and *Nr3c1*$^{fl/fl}$*Cd4*-cre$^+$ (GRcKO) mice after 3 hours of culture without IL-7 ($n$ = 3–4). (**F**) Flow cytometry of Bcl2 expression in CD4$^+$ T and CD8$^+$ T cells in spleens of *Nr3c1*$^{fl/fl}$ (control) and *Nr3c1*$^{fl/fl}$*Cd4*-cre$^+$ (GRcKO) mice at ZT16. (**G**) qPCR analysis of *Bcl2* and *Bclxl* mRNA of CD4$^+$ T and CD8$^+$ T cells in spleens of *Nr3c1*$^{fl/fl}$ (control) and *Nr3c1*$^{fl/fl}$*Cd4*-cre$^+$ (GRcKO) mice at ZT16 ($n$ = 4). (**H**) qPCR analysis of *Bcl2* and *Bclxl* mRNA of CD4$^+$ SP and CD8$^+$ SP thymocytes from *Nr3c1*$^{fl/fl}$ (control) and *Nr3c1*$^{fl/fl}$*Cd4*-cre$^+$ (GRcKO) mice at ZT16 ($n$ = 4). (**I**) Bcl2 expression in CD4$^+$ T and CD8$^+$ T cells in spleens of wild-type (WT) and *Il7r*$^{CNS1.GRE12m/12m}$ (GRE12m, GR12) mice at ZT16 was analyzed by flow cytometry. (**J**) qPCR analysis of *Bcl2* and *Bclxl* mRNA of CD4$^+$ T and CD8$^+$ T cells in spleens of wild-type and GRE12m mice at ZT16 ($n$ = 4). (**K**) qPCR analysis of *Bcl2* and *Bclxl* mRNA in CD4$^+$ SP and CD8$^+$ SP thymocytes from wild-type (WT) and GRE12m (GR12) mice at ZT16 ($n$ = 4). All data are pooled from two to three independent experiments. Data are means ± SEM. Student's $t$-test, *$p < 0.05$, **$p < 0.01$, ***$p < 0.001$.

**Figure S5, related to Figure 3: CXCR4 deficiency does not affect T cell survival.**

(**A**) CD44, CD62L, CCR7, and CD11a expression levels were analyzed by flow cytometry at ZT16 in CD4$^+$ T and CD8$^+$ T cells of spleen from *Nr3c1*$^{fl/fl}$ (control) and *Nr3c1*$^{fl/fl}$*Cd4*-cre$^+$ (GRcKO) mice. (**B**) Surface IL-7R expression in CD4 T and CD8 T cells of spleen from *Cxcr4*$^{fl/fl}$ (control) and *Cxcr4*$^{fl/fl}$*Cd4*-cre$^+$ (CXCR4cKO) mice at ZT16. (**C**) Bcl2 expression

was analyzed by flow cytometry in $CD4^+$ T and $CD8^+$ T cells of spleen from *Cxcr4*$^{fl/fl}$ (control) and *Cxcr4*$^{fl/fl}$*Cd4*-cre$^+$ (CXCR4cKO) mice at ZT16. (**D**) Naive $CD4^+$ T cells in lymph nodes of C57BL/6 ($CD45.1^+$) and *Cxcr4*$^{fl/fl}$ (control) or *Cxcr4*$^{fl/fl}$*Cd4*-cre$^+$ (CXCR4cKO) ($CD45.2^+$) mice were purified at ZT4, mixed at a 1:1 ratio, labeled with CFSE, and transferred into C57BL/6 ($CD45.2^+$) mice ($5 \times 10^6$ cells in total). After 8 days, $CFSE^+$ donor cells were analyzed at ZT4 in spleen, lymph nodes (LN), and peripheral blood. Percentages of $CD45.2^+$ and $CD45.2^-$ cells in $CFSE^+$ $CD4^+$ T cells are shown ($n$ = 3). (**E**) Mice were injected with dexamethasone at ZT0. Expression of IL-7R and CXCR4 (mean fluorescence intensity, MFI) and the numbers of splenic $CD4^+$ T cells after 4 hours of dexamethasone administration *in vivo* at ZT4 ($n$ = 3). (**F**) Mice were injected with 10 μg IL-7 at ZT0 or ZT8, respectively. Expression of CXCR4 of splenic $CD4^+$ T cells after 4 hours of intravenous IL-7 administration *in vivo* at ZT4 or ZT12. (**G**) Naïve $CD4^+$ T cells were purified from spleen at ZT4 or ZT8, and stimulated with or without IL-7 (10 ng/ml) for 10 and 20 hours in vitro. CXCR4 expression was analyzed by flow cytometry. All data are pooled from two to three independent experiments. Data are means ± SEM. Student's *t*-test, *$p < 0.05$, **$p < 0.01$, n.s. not significant.

**Figure S6, related to Figure 4: CXCR4 induces T cell migration into the CXCL12-expressing T cell zone.**

(**A**–**C**) Immunohistochemistry of Peyer's patches from *Cxcl12*-GFP mice (A and B) or *Il7*-GFP mice (C). Wild-type T cells were isolated from lymph nodes at ZT16, labeled with CellTracker Deep Red (A and B) or CMTMR (C), and transferred at ZT18 into *Cxcl12*-GFP or *Il7*-GFP mice. After 1 hour, anti-B220, anti-TCRβ, and anti-CD31 antibodies were used to detect the B cell zone, T cell zone, and vessels, respectively. Scale bars, 100 μm. (**D**) Immunohistochemistry of Peyer's patches from *Cxcl12*-GFP mice. T cells from *Nr3c1*$^{fl/fl}$

(control) and *Nr3c1*$^{fl/fl}$*Cd4*-cre$^{+}$ (GRcKO) mice were isolated from lymph nodes at ZT16 and labeled with CellTracker Deep Red (blue) and CMTMR (red), respectively, mixed in equal proportions, and transferred at ZT18 into *Cxcl12*-GFP mice. After 1 hour, anti-TCRβ antibody (cyan) was used to detect the T cell zone. Scale bar, 100 μm. (**E**) Percentage of *Nr3c1*$^{fl/fl}$ (control) and *Nr3c1*$^{fl/fl}$*Cd4*-cre$^{+}$ (GRcKO) T cells among total labeled cells present within Peyer's patches in (D) ($n$ = 4). All data are pooled from two independent experiments. Data are means ± SEM. Student's $t$-test, *$p < 0.05$.

**Figure S7, related to Figures 5 and 6: GRs control differentiation of Th subsets and immune response of B cells.**

(A) Naïve CD4$^{+}$ and CD8$^{+}$ T cells were isolated from spleen of *Nr3c1*$^{fl/fl}$ (control) and *Nr3c1*$^{fl/fl}$*Cd4*-cre$^{+}$ (GRcKO), wild-type (WT), and *Il7r*$^{CNS1.GRE12m/12m}$ (GRE12m, GR12) mice, at ZT4 and ZT16 and stimulated with anti-CD3 and CD28 antibodies for 96 hours. Proliferation was assessed by CFSE dilution assay. Gates were set for the divided cells and the cells with more than 4 times divisions. Percentage of each cell population was shown ($n$ = 3). (**B**) Naïve CD4$^{+}$ and CD8$^{+}$ T cells were isolated from lymph nodes of wild-type (WT) and *Il7r*$^{CNS1.GRE12m/12m}$ (GRE12m, GR12) mice at ZT16. The cells were labeled with CFSE, and cultured with anti-CD3 antibody, anti-CD28 antibody, and human IL-2 for 96 hours (upper panels). The cells were stimulated with anti-CD3 and anti-CD28 antibodies for 48 hours, and their IL-2R expression was assessed (middle and lower panels). (**C**) Intracellular cytokine staining in naive CD4$^{+}$ T cells of *Nr3c1*$^{fl/fl}$ (control, Ctrl) and *Nr3c1*$^{fl/fl}$*Cd4*-cre$^{+}$ (GRcKO) mice, isolated from lymph nodes at ZT16 and cultured under Th1 and Th2 conditions. (**D**) Frequency of IFN-γ$^{+}$ cells under Th1 conditions and IL-4$^{+}$ and IL-13$^{+}$ cells under Th2 conditions ($n$ = 6–7). Naive CD4$^{+}$ T cells were isolated from lymph nodes at ZT4 and ZT16. (**E**) E4BP4 and GATA3 expression in CD4$^{+}$ T cells isolated from lymph nodes at ZT16 and

cultured under Th2 conditions for 48 hours. (**F** and **G**) *Nr3c1*$^{fl/fl}$ (control) and *Nr3c1*$^{fl/fl}$*Cd4*-cre$^{+}$ (GRcKO) mice were immunized with OVA at ZT16. One week after injection, spleen cells were isolated at ZT16 and stimulated with OVA for 3 days. Protein levels of IL-4 and IL-13 in supernatant ($n$ = 4) (F) and mRNA levels of IL-4 and IL-13 in sorted PD-1$^{+}$CXCR5$^{+}$ follicular helper T (Tfh) cells (G) ($n$ = 6). (**H**) Intracellular cytokine staining in naïve CD4$^{+}$ T cells of wild-type (WT), and *Il7r*$^{CNS1.GRE12m/12m}$ (GRE12m, GR12) mice, isolated from lymph nodes at ZT16 and cultured for IFN-γ and IL-2 under Th1 conditions and for IL-4 and IL-13 under Th2 conditions. (**I**) Wild-type (WT), and *Il7r*$^{CNS1.GRE12m/12m}$ (GRE12m, GR12) mice were immunized with OVA at ZT4 or ZT16. After 12 days (288 hours), CXCR5$^{+}$PD-1$^{+}$ follicular helper T cells (Tfh), GL7$^{+}$CD95$^{+}$ germinal-center B cells, and IgG1$^{+}$ B cells were analyzed in spleen at ZT4 or ZT16, respectively, by flow cytometry ($n$ = 3–8). (**J**) Numbers of CXCR5$^{+}$PD-1$^{+}$ Tfh cells, GL7$^{+}$CD95$^{+}$ germinal center B cells, and IgG1$^{+}$ B cells in Peyer's patches of wild-type (WT), and *Il7r*$^{CNS1.GRE12m/12m}$ (GRE12m, GR12) mice at ZT16 ($n$ = 4). All data are pooled from two to four independent experiments. Data are means ± SEM. Student's $t$-test, *$p < 0.05$, **$p < 0.01$.

**KEY RESOURCES TABLE**

| REAGENT or RESOURCE | SOURCE | IDENTIFIER |
|---|---|---|
| Antibodies | | |
| Anti-mouse CD3ε (145-2C11)-FITC | TONBO Biosciences | Cat#35-0031 |
| Anti-mouse CD3ε (145-2C11) | In house | N/A |
| Anti-mouse TCRβ (H57-597)-FITC | BioLegend | Cat#109206;RRID:AB_313429 |
| Anti-mouse TCRβ (H57-597)-biotin | BioLegend | Cat#109204;RRID:AB_313427 |
| Anti-mouse CD4 (RM4-5)-APC-eFluor 780 | eBioscience | Cat#47-0042; RRID:AB_1272183 |
| Anti-mouse CD8a (53-6.7)-eFluor 450 | eBioscience | Cat#48-0081; RRID:AB_1272198 |
| Anti-mouse CD8a (53-6.7)-PE-Cy7 | TONBO Biosciences | Cat#60-0081 |
| Anti-mouse CD11a (M17/4)-PE | BioLegend | Cat#101107; RRID:AB_312780 |
| Anti-mouse CD25 (PC61.5)-APC | TONBO Biosciences | Cat#20-0251; |
| Anti-human/mouse CD44 (IM7)-PE-Cy7 | eBioscience | Cat#25-0441; RRID:AB_469622 |
| Anti-mouse NK1.1 (PK136)-PE-Cy7 | BioLegend | Cat#108714; RRID:AB_389364 |
| Anti-mouse NK1.1 PE (PK136)-PE | TONBO Biosciences | Cat#50-5941 |
| Anti-mouse CD69 (H1.2F3)-PE | eBioscience | Cat#12-0691; RRID:AB_465731 |
| Anti-mouse PD-1 (29F.1A12)-APC | BioLegend | Cat#135209; RRID:AB_2159183 |
| Anti-mouse CXCR4 (L276F12)-biotin | BioLegend | Cat#146516; RRID:AB_2056787 |
| Rat IgG2b, κ, isotype control (RTK4530)-biotin | BioLegend | Cat#400604 |
| Anti-mouse CXCR5 (L138D7)-biotin | BioLegend | Cat#145519; RRID:AB_2562865 |
| Anti-mouse CCR7 (4B12)-PE | BioLegend | Cat#120105; RRID:AB_389357 |
| Anti-mouse CD62L (MEL-14)-APC | BioLegend | Cat#104411; RRID:AB_313098 |
| Anti-mouse CD95 (15A7)-biotin | eBioscience | Cat#13-0951-81; RRID:AB_466544 |
| Anti-human/mouse GL7 antigen (GL7)-PE | BioLegend | Cat#144607; RRID:AB_2562925 |
| Anti-human/mouse B220 (RA3-6B2)-APC-eFluor 780 | eBioscience | Cat#47-0452; RRID:AB_1518810 |
| Anti-human/mouse B220 (RA3-6B2)-biotin | TONBO Biosciences | Cat#30-0452 |
| Anti-mouse CD19 (6D5)-PE-Cy7 | BioLegend | Cat#115520; RRID:AB_313655 |
| Anti-mouse CD19 (6D5)-Alexa Fluor 488 | BioLegend | Cat#115521; RRID:AB_389307 |
| Anti-mouse IgG1 (RMG1-1)-APC | BioLegend | Cat#406609; RRID:AB_10679040 |
| Anti-mouse IFNγ (XMG1.2)-FITC | eBioscience | Cat#11-7311; RRID:AB_465412 |
| Anti-mouse IFNγ (AN-18) | BioLegend | Cat#517901; RRID:AB_10900809 |

| | | |
|---|---|---|
| Anti-mouse IL-2 (JES6-5H4)-APC | BioLegend | Cat#503809; RRID:AB_315303 |
| Anti-mouse IL-4 (11B11)-Alexa Fluor 488 | BioLegend | Cat#504111; RRID:AB_493321 |
| Anti-mouse IL-4 (11B11) | TONBO Biosciences | Cat#70-7041 |
| Anti-mouse IL-13 (eBio13A)-PE | eBioscience | Cat#12-7133; RRID:AB_763559 |
| Anti-mouse E4BP4 (S2M-E19)-PE | eBioscience | Cat#12-5927; RRID:AB_11149135 |
| Anti-mouse GATA3 (16E10A23)-APC | BioLegend | Cat#653805; RRID:AB_2562724 |
| Anti-mouse CD45.2 (104)-APC | eBioscience | Cat#17-0454; RRID:AB_469400 |
| Anti-mouse CD122 (TM-beta1)-biotin | Dr. Masayuki Miyasaka, in house | N/A |
| Anti-mouse CD127 (A7R34)-biotin | BioLegend | Cat#135006; RRID:AB_2126118 |
| Rat IgG2a, κ, isotype control (RTK2758)-biotin | BioLegend | Cat#400504 |
| Anti-mouse STAT5-pY694 (47)-PE | BD biosciences | Cat#612567 |
| Anti-mouse IgG1 isotype-PE | BD biosciences | Cat#555749 |
| Anti-mouse Bcl-2 set PE | BD biosciences | Cat#556537 |
| Anti-mouse CD31 (MEC13.3)-PE | Biolegend | Cat#102507; RRID:AB_312914 |
| Anti-mouse CD31 (MEC13.3)-FITC | Biolegend | Cat#102506; RRID:AB_312913 |
| Anti-mouse CD31 (MEC13.3)-Alexa Fluor 647 | Biolegend | Cat#102515; RRID:AB_2161030 |
| Rabbit anti-GFP | Invitrogen | Cat#A-11122; RRID:AB_221569 |
| Anti-rabbit IgG (Poly4064)-DyLight 649 | Biolegend | Cat#406406; RRID:AB_1575135 |
| Anti-mouse CD28 (PV-1) | Gift from Dr. Ryo Abe | N/A |
| Streptavidin-PE | eBioscience | Cat#12-4312-87 |
| Streptavidin-Brilliant Violet 421 | BioLegend | Cat#405225 |
| SBA clonotyping system-HRP | Southern Biotech | Cat#5300-05 |
| Anti-glucocorticoid receptor mouse mAb (BuGR2) | Merck | Cat#GR32L-100UGCN |
| Whole mouse IgG | Jackson ImmunoResearch | Cat#015-000-003 |
| Bacterial and Virus Strains | | |
| *Listeria monocytogenes*: OVA-expressing recombinant, rLM-OVA | Dr. Yasunobu Yoshikai, originally from Dr. Leo Lefrancois | (Pope et al., 2001) |
| AxCANCre: Cre-expressing adenovirus, AdV-Cre | Dr. Izumu Saito | (Kanegae et al., 1995) |
| Chemicals, Peptides, and Recombinant Proteins | | |
| Recombinant mouse IL-7 | BioLegend | Cat#577806 |
| Recombinant mouse CXCL12 | TONBO Biosciences | Cat#21-8141 |
| Recombinant mouse IL-4 | BioLegend | Cat#588204 |
| Recombinant mouse IL-12 | PeproTech | Cat#210-12 |
| Recombinant human IL-2 | BioLegend | Cat#589102 |
| PMA | Cayman | Cat#10008014 |

| | | |
|---|---|---|
| Ionomycin | Cayman | Cat#10004974 |
| Brefeldin A | Cayman | Cat#11861 |
| 5-(and -6)-Carboxyfluorescein diacetate succinimidyl ester (CFSE) | Dojindo | Cat#341-07401 |
| 5-(6)-(((4-Chloromethyl)Benzoyl)Amino)Tetramethylrhodamine (CMTMR) | Setareh Biotech | Cat#7138 |
| CellTracker Deep Red | Thermo Fisher Scientific | Cat#C34565 |
| Dexamethasone | Sigma-Aldrich | Cat#D4092 |
| Dexamethasone 21-phosphate disodium salt | Sigma-Aldrich | Cat#D1159 |
| Albumin from chicken egg white (OVA) | Sigma-Aldrich | Cat#A5503 |
| Bovine serum albumin (BSA) | Nacalai Tesque | Cat#08587-26 |
| NP-OVAL | LGC Biosearch Technologies | Cat#N-5051-10 |
| NP-BSA | LGC Biosearch Technologies | Cat#N-5050H-10 |
| Imject Alum Adjuvant | Thermo Fisher Scientific | Cat#77161 |
| DNase I | Worthington Biochemical | Cat#DT |
| Collagenase D | Sigma-Aldrich | Cat#11088882001 |
| Percoll | GE Healthcare | Cat#17-0891-01 |
| ABTS | Sigma-Aldrich | Cat#10102946001 |
| RPMI 1640 Medium | Nacalai Tesque | Cat#30246-85 |
| FBS | ICN Biomedicals | Cat#29-167-54 |
| Sepasol RNA I SuperG | Nacalai Tesque | Cat#09379-97 |
| Recombinant DNase I (RNase-free) | Takara Bio | Cat#2270A |
| RNase Inhibitor | Takara Bio | Cat#2313A |
| ReverTra Ace | TOYOBO | Cat#TRT-101 |
| Random Primers | Invitrogen | Cat#48190-011 |
| ROX Reference Dye | Invitrogen | Cat#12223-012 |
| Critical Commercial Assays | | |
| Foxp3 Staining Buffer Set | eBioscience | Cat#00-5523-00 |
| IC Fixation Buffer | eBioscience | Cat#00-8222-49 |
| EasySep Mouse Naïve CD4+ T Isolation Kit | STEMCELL Technologies | Cat#ST19765 |
| EasySep Mouse Naïve CD8+ T Isolation Kit | STEMCELL Technologies | Cat#ST19858 |
| Pan T Cell Isolation Kit II, mouse | Miltenyi Biotech | Cat#130-095-130 |
| CaspGLOW Fluorescein Active Caspase-3 Staining kit | Thermo Fisher Scientific | Cat#88-7004-42 |
| QuikChange Site-Directed Mutagenesis Kit | Agilent Technologies | Cat#200519 |
| Mouse IL-4 ELISA Ready-SET-Go Kit | eBioscience | Cat#88-7044-22 |
| Mouse IL-13 ELISA Ready-SET-Go Kit | eBioscience | Cat#88-7137-22 |
| Transwell 24 well, 6.5 mm diameter, 5 μm pore | Corning | Cat#3421 |
| T-select MHC I Tetramer (H-2Kb OVA Tetramer APC) | Medical & Biological Laboratories | Cat#TS-5001-2C |
| Protein G Sepharose 4 Fast Flow | GE Healthcare | Cat#17061802 |
| QuantiTect SYBR Green PCR Kit | QIAGEN | Cat#204145 |
| Experimental Models: Organisms/Strains | | |

| | | |
|---|---|---|
| Mouse: C57BL/6 | Japan SLC<br>CLEA Japan | C57BL/6 |
| Mouse: C57BL/6-CD45.1: B6.SJL-*Ptprc*$^{a}$ *Pepc*$^{b}$/BoyJ | Dr. Irving L. Weissman | JAX:002014 |
| Mouse: *CD4*-cre: B6.Cg-Tg(Cd4-cre)1Cwi | Dr. Christopher B. Wilson | JAX:022071 |
| Mouse: *Nr3c1*$^{fl/fl}$: B6.129-*Nr3c1*$^{tm2Gsc}$, | Dr. Günther Schütz | EM:02124 |
| Mouse: *Il7r*$^{fl/fl}$: B6.129-*Il7r*$^{tm2Iku}$ | Lab of Koichi Ikuta | N/A |
| Mouse: *Cxcr4*$^{fl/fl}$: B6.129-*Cxcr4*$^{tm2Tng}$ | Dr. Takashi Nagasawa | RBRC:04198 |
| Mouse: *Cxcl12*-GFP: B6.129-*Cxcl12*$^{tm2Tng}$ | Dr. Takashi Nagasawa | RBRC:04200 |
| Mouse: *Il7*–GFP: B6.129-*Il7*$^{tm1.1Iku}$ | Lab of Koichi Ikuta | N/A |
| Mouse: GRE1m: $Il7r^{CNS1.GRE1m/1m}$ | This paper | N/A |
| Mouse: GRE2m: $Il7r^{CNS1.GRE2m/2m}$ | This paper | N/A |
| Mouse: GRE12m: $Il7r^{CNS1.GRE12m/12m}$ | This paper | N/A |
| Oligonucleotides | | |
| Gapdh primer:<br>F: CCTCGTCCCGTAGACAAAATG;<br>R: TCTCCACTTTGCCACTGCAA | This paper | N/A |
| IL-7R primer:<br>F: GGATGGAGACCTAGAAGATG;<br>R: GAGTTAGGCATTTCACTCGT | This paper | N/A |
| CXCR4 primer:<br>F: TGTTGCCATGGAACCGATCA;<br>R: TGGTGGGCAGGAAGATCCTA | This paper | N/A |
| Bcl2 primer:<br>F: TCGCTACCGTCGTGACTTC;<br>R: AAACAGAGGTCGCATGCTG | This paper | N/A |
| BclxL primer:<br>F: GGAGAGCGTTCAGTGATC;<br>R: CAATGGTGGCTGAAGAGA | This paper | N/A |
| IL-4 primer:<br>F: AGGAGCCATATCCACGGATG;<br>R: ACAGACGAGCTCACTCTCTG | This paper | N/A |
| IL-13 primer:<br>F: CAGCTCCCTGGTTCTCTCAC;<br>R: ACACTCCATACCATGCTGCC | This paper | N/A |
| Primers for 5' homologous fragment of the targeting vector, see Experimental Procedures and Figure S2:<br>F: TCTTATGGAGGCTTTGGAGG<br>R: GAGTCTTTGGGCACCTGAGA | This paper | N/A |
| Primers for 3' homologous fragment of the targeting vector, see Experimental Procedures and Figure S2:<br>F: CTTTTTTCATCTTCCTTTCAAAC<br>R: ATGTCACTTGAGTGGCAGAC | This paper | N/A |
| Primers for probe A, see Experimental Procedures and Figure S2:<br>F: TACCAACTTTGAAGCTGCTG<br>R: CCTCCAAAGCCTCCATAAGA | This paper | N/A |
| Primers for probe B, see Experimental Procedures and Figure S2:<br>F: TGCAAAGGAAGGAGTGTCTG<br>R: GCACATACATATGCTTGTGG | This paper | N/A |
| Software and Algorithms | | |
| FlowJo v10.2 | Tree Star | RRID:SCR_008520 |
| GraphPad Prism 7.0 | GraphPad Software | RRID:SCR_002798 |

| | | |
|---|---|---|
| Leica LAS AF image acquisition software | Leica Microsystems | RRID:SCR_013673 |

# Figure 1

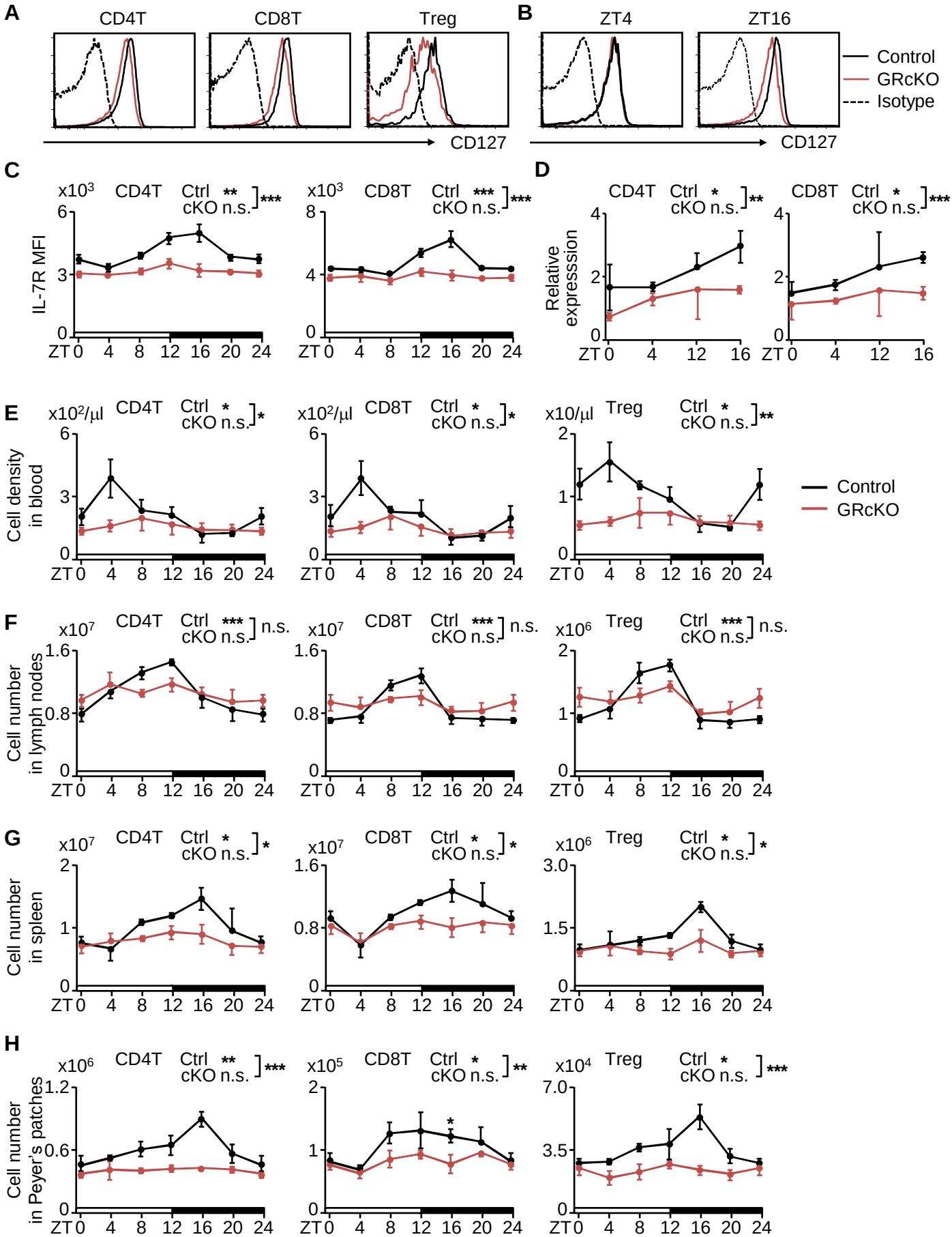
A
CD4T
CD8T
Treg
CD127
B
ZT4
ZT16
CD127
Control
GRcKO
Isotype
C
x10³ CD4T Ctrl ** cKO n.s. ]***
x10³ CD8T Ctrl *** cKO n.s. ]***
IL-7R MFI
ZT 0 4 8 12 16 20 24
D
CD4T Ctrl * cKO n.s. ]**
CD8T Ctrl * cKO n.s. ]***
Relative expresssion
ZT 0 4 12 16
E
x10²/µl CD4T Ctrl * cKO n.s. ]*
x10²/µl CD8T Ctrl * cKO n.s. ]*
x10/µl Treg Ctrl * cKO n.s. ]**
Cell density in blood
Control
GRcKO
F
x10⁷ CD4T Ctrl *** cKO n.s. ] n.s.
x10⁷ CD8T Ctrl *** cKO n.s. ] n.s.
x10⁶ Treg Ctrl *** cKO n.s. ] n.s.
Cell number in lymph nodes
G
x10⁷ CD4T Ctrl * cKO n.s. ]*
x10⁷ CD8T Ctrl * cKO n.s. ]*
x10⁶ Treg Ctrl * cKO n.s. ]*
Cell number in spleen
H
x10⁶ CD4T Ctrl ** cKO n.s. ]***
x10⁵ CD8T Ctrl * cKO n.s. ]**
x10⁴ Treg Ctrl * cKO n.s. ]***
Cell number in Peyer's patches

# Figure 2

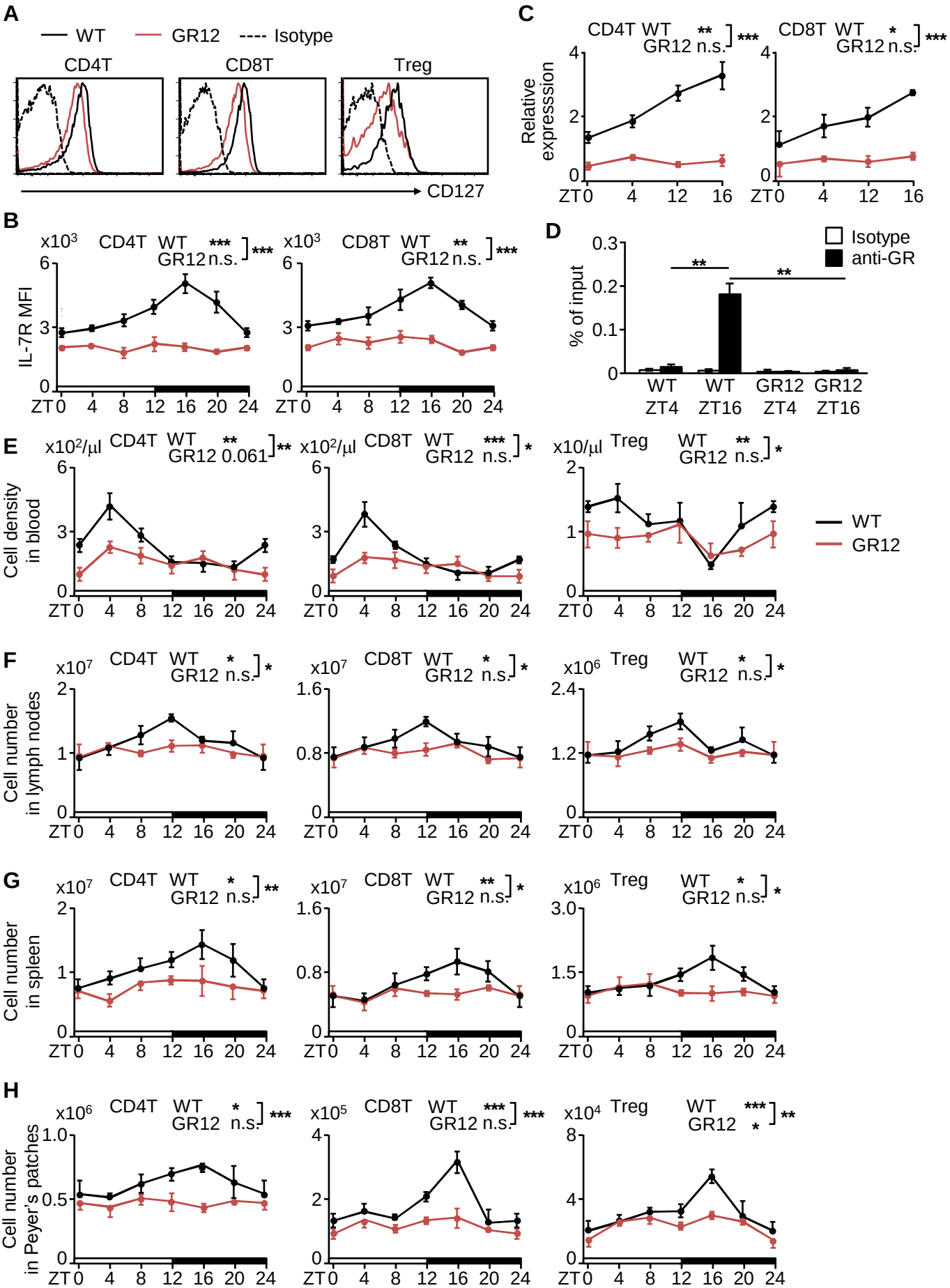
A
WT
GR12
Isotype
CD4T
CD8T
Treg
CD127
B
x10³ CD4T WT GR12 *** n.s. ***
x10³ CD8T WT GR12 ** n.s. ***
IL-7R MFI
ZT 0 4 8 12 16 20 24
C
CD4T WT GR12 ** n.s. ***
CD8T WT GR12 * n.s. ***
Relative expresssion
ZT 0 4 12 16
D
Isotype
anti-GR
% of input
WT ZT4
WT ZT16
GR12 ZT4
GR12 ZT16
E
x10²/μl CD4T WT GR12 ** 0.061 **
x10²/μl CD8T WT GR12 *** n.s. *
x10/μl Treg WT GR12 ** n.s. *
Cell density in blood
WT
GR12
F
x10⁷ CD4T WT GR12 * n.s. *
x10⁷ CD8T WT GR12 * n.s. *
x10⁶ Treg WT GR12 * n.s. *
Cell number in lymph nodes
G
x10⁷ CD4T WT GR12 * n.s. **
x10⁷ CD8T WT GR12 ** n.s. *
x10⁶ Treg WT GR12 * n.s. *
Cell number in spleen
H
x10⁶ CD4T WT GR12 * n.s. ***
x10⁵ CD8T WT GR12 *** n.s. ***
x10⁴ Treg WT GR12 *** * **
Cell number in Peyer's patches

# Figure 3

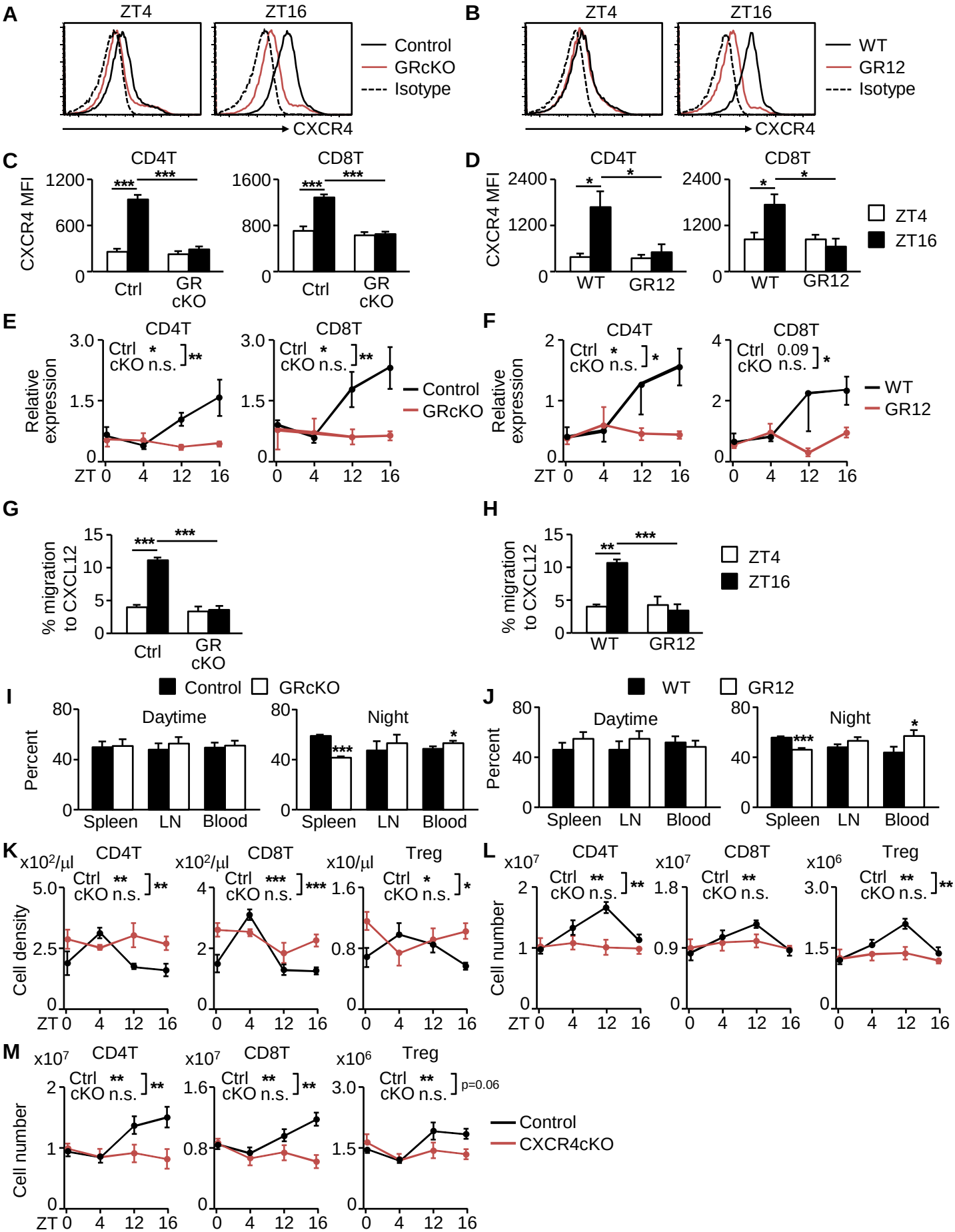
A
ZT4
ZT16
Control
GRcKO
Isotype
CXCR4
B
ZT4
ZT16
WT
GR12
Isotype
CXCR4
C
CD4T
CD8T
CXCR4 MFI
Ctrl
GR cKO
D
CD4T
CD8T
CXCR4 MFI
WT
GR12
ZT4
ZT16
E
CD4T
CD8T
Relative expression
Ctrl
cKO
n.s.
Control
GRcKO
ZT
F
CD4T
CD8T
Relative expression
Ctrl
cKO
n.s.
0.09
WT
GR12
G
% migration to CXCL12
Ctrl
GR cKO
H
% migration to CXCL12
WT
GR12
ZT4
ZT16
I
Control
GRcKO
Daytime
Night
Percent
Spleen
LN
Blood
J
WT
GR12
Daytime
Night
Percent
Spleen
LN
Blood
K
CD4T
CD8T
Treg
Cell density
Ctrl
cKO
n.s.
ZT
L
CD4T
CD8T
Treg
Cell number
Ctrl
cKO
n.s.
ZT
M
CD4T
CD8T
Treg
Cell number
Ctrl
cKO
n.s.
p=0.06
Control
CXCR4cKO
ZT

# Figure 4

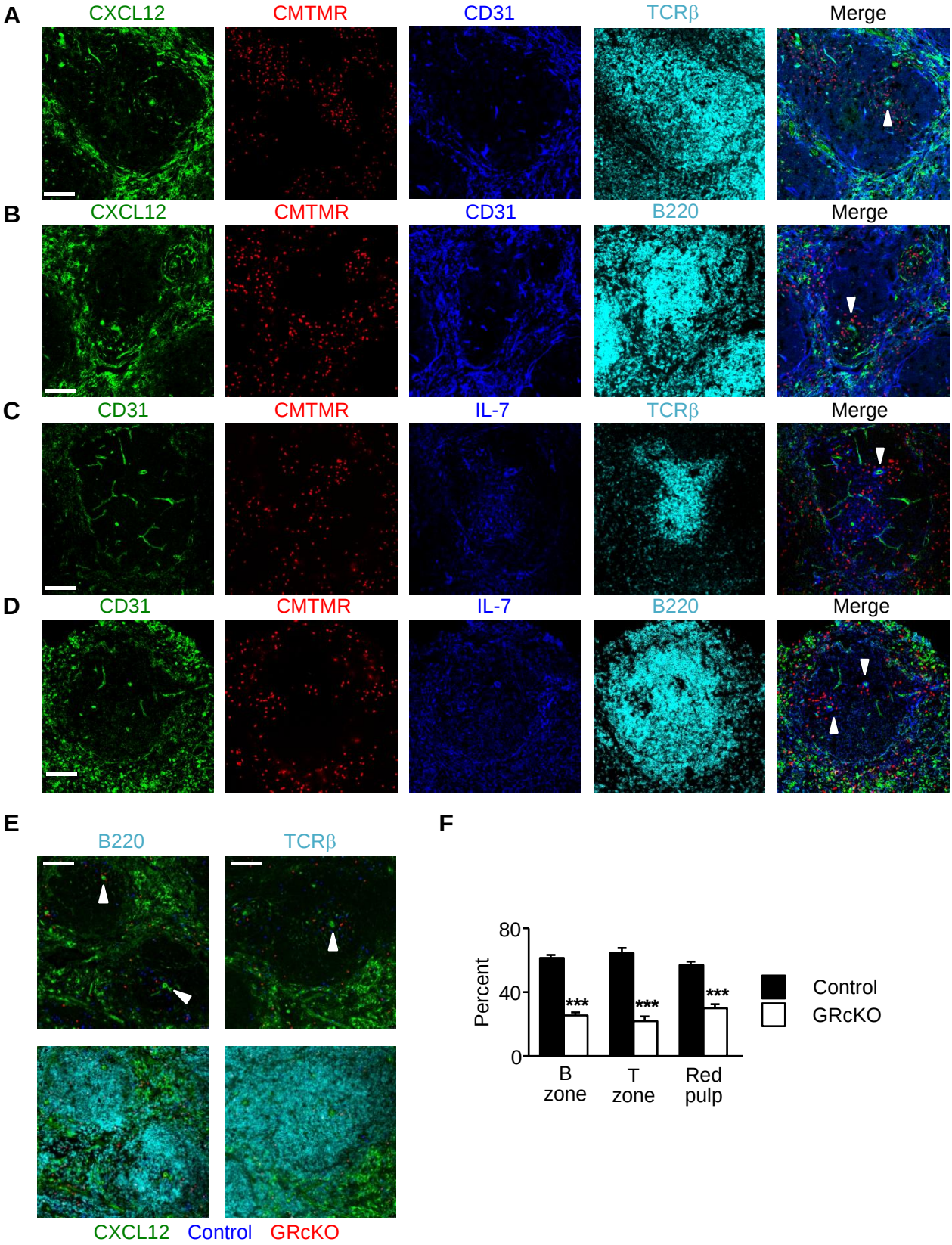
A
CXCL12
CMTMR
CD31
TCRβ
Merge
B
CXCL12
CMTMR
CD31
B220
Merge
C
CD31
CMTMR
IL-7
TCRβ
Merge
D
CD31
CMTMR
IL-7
B220
Merge
E
B220
TCRβ
CXCL12
Control
GRcKO
F
Percent
80
40
0
***
***
***
B zone
T zone
Red pulp
Control
GRcKO

# Figure 5

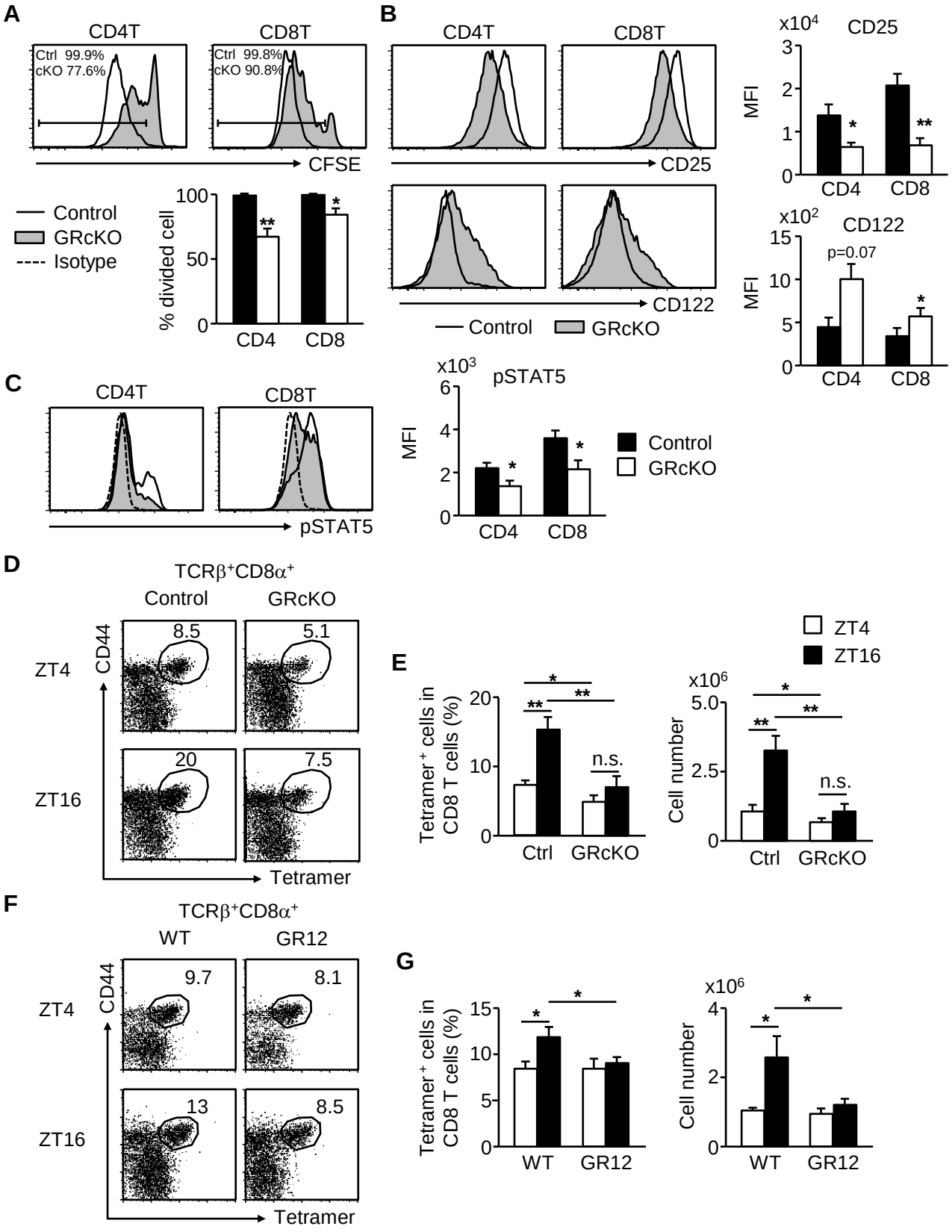
A
CD4T
CD8T
Ctrl 99.9%
cKO 77.6%
Ctrl 99.8%
cKO 90.8%
CFSE
Control
GRcKO
Isotype
% divided cell
100
50
0
CD4
CD8
B
CD4T
CD8T
CD25
CD122
Control
GRcKO
x10^4
CD25
MFI
3
2
1
0
CD4
CD8
x10^2
CD122
p=0.07
15
10
5
0
C
CD4T
CD8T
pSTAT5
x10^3
pSTAT5
6
4
2
0
D
TCRβ+CD8α+
Control
GRcKO
ZT4
ZT16
CD44
8.5
5.1
20
7.5
Tetramer
E
ZT4
ZT16
Tetramer+ cells in CD8 T cells (%)
20
10
0
n.s.
Ctrl
GRcKO
x10^6
Cell number
5.0
2.5
0
F
TCRβ+CD8α+
WT
GR12
9.7
8.1
13
8.5
G
15
10
5
4
2

# Figure 6

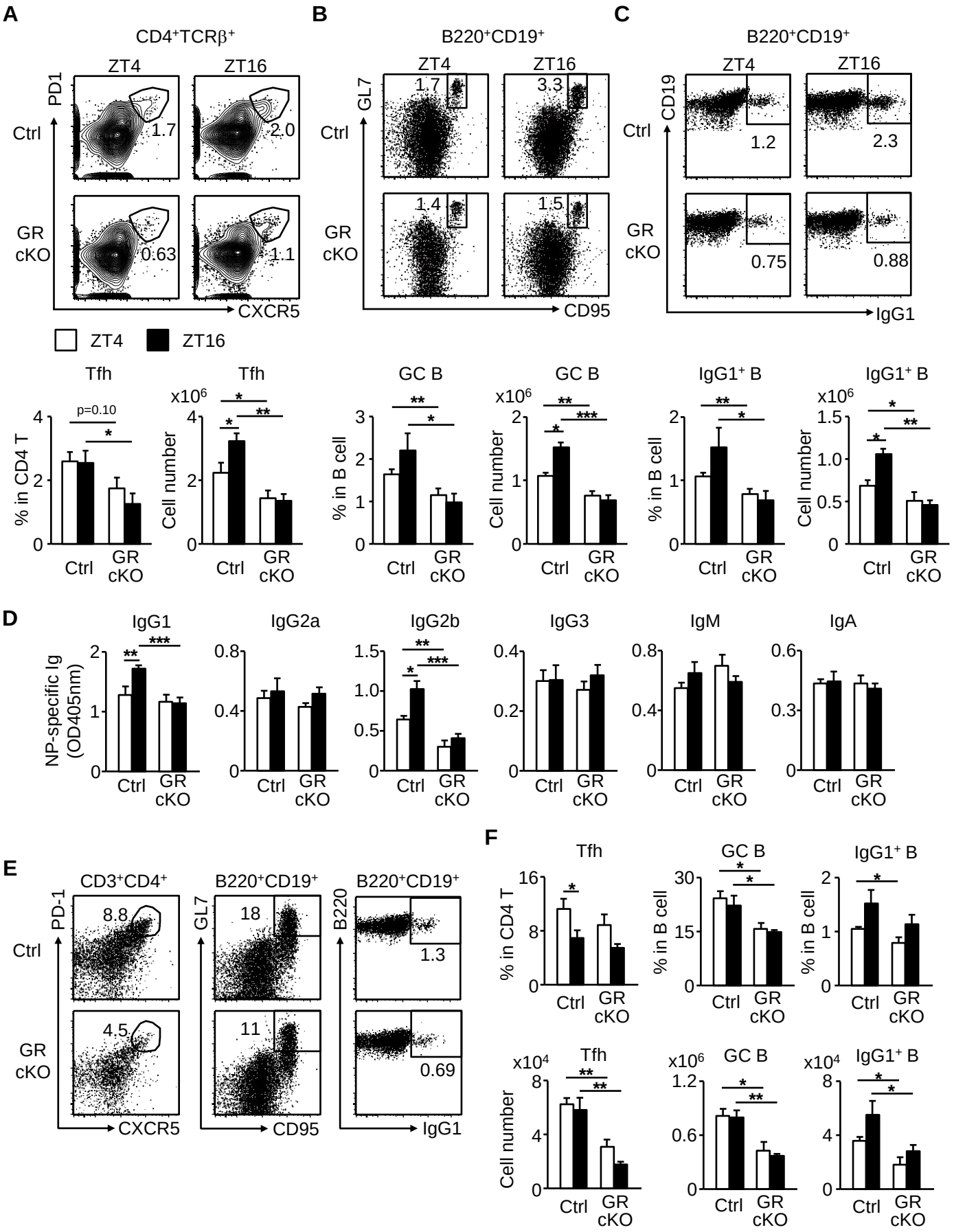
A
CD4+TCRβ+
ZT4
ZT16
PD1
Ctrl
GR cKO
1.7
2.0
0.63
1.1
CXCR5
ZT4
ZT16
B
B220+CD19+
GL7
1.7
3.3
1.4
1.5
CD95
C
B220+CD19+
CD19
1.2
2.3
0.75
0.88
IgG1
ZT4
ZT16
Tfh
% in CD4 T
p=0.10
Tfh
x10^6
Cell number
GC B
% in B cell
GC B
x10^6
Cell number
IgG1+ B
% in B cell
IgG1+ B
x10^6
Cell number
Ctrl
GR cKO
D
IgG1
IgG2a
IgG2b
IgG3
IgM
IgA
NP-specific Ig (OD405nm)
Ctrl
GR cKO
E
CD3+CD4+
PD-1
8.8
4.5
CXCR5
B220+CD19+
GL7
18
11
CD95
B220+CD19+
B220
1.3
0.69
IgG1
F
Tfh
% in CD4 T
GC B
% in B cell
IgG1+ B
% in B cell
Tfh
x10^4
Cell number
GC B
x10^6
IgG1+ B
x10^4
Ctrl
GR cKO

# Figure 7

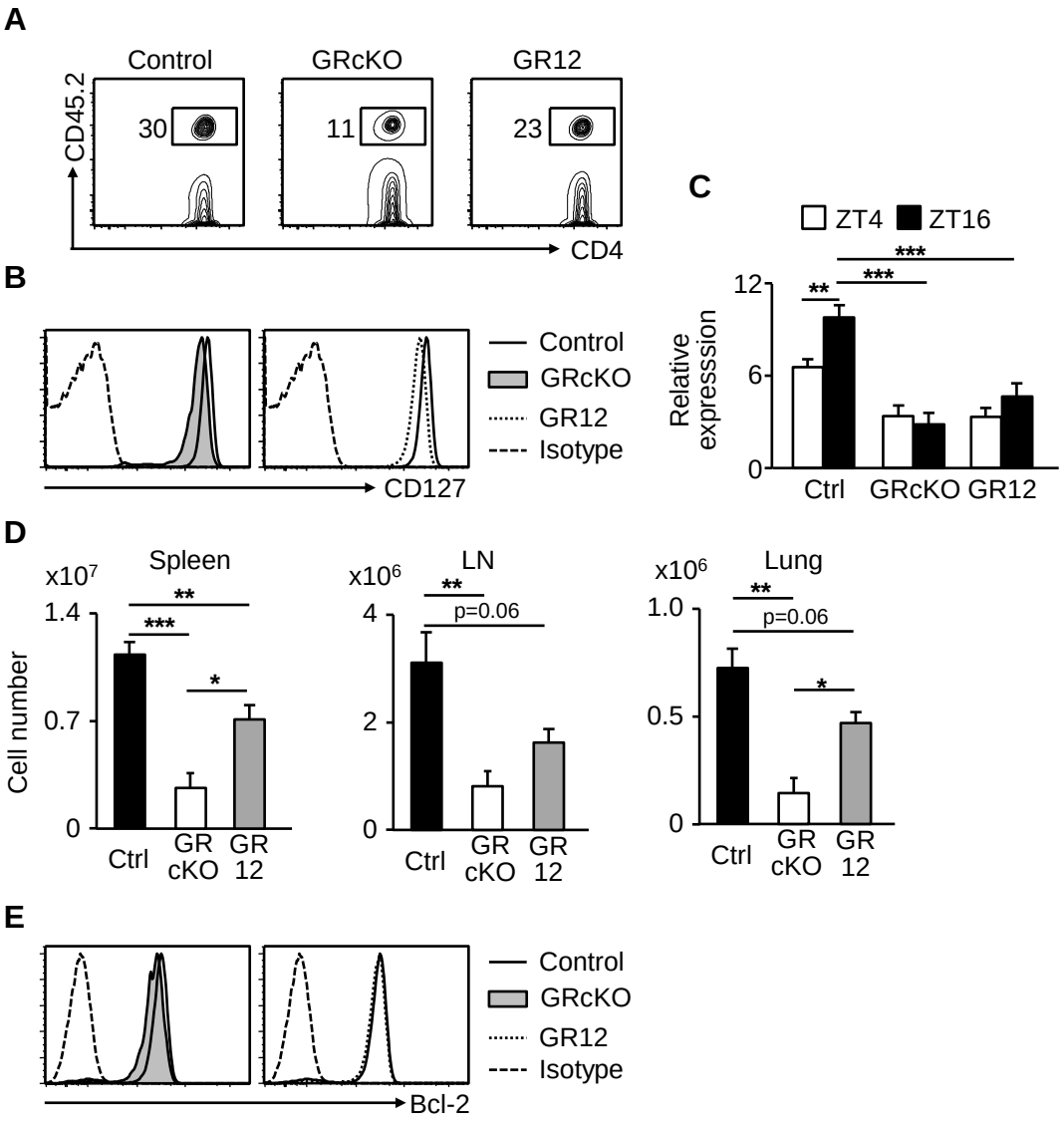
A
Control
GRcKO
GR12
CD45.2
30
11
23
CD4
B
Control
GRcKO
GR12
Isotype
CD127
C
ZT4
ZT16
***
**
***
12
6
0
Relative expresssion
Ctrl
GRcKO
GR12
D
Spleen
x10^7
1.4
0.7
0
Cell number
**
***
*
Ctrl
GR cKO
GR 12
LN
x10^6
4
2
0
**
p=0.06
Lung
x10^6
1.0
0.5
0
E
Control
GRcKO
GR12
Isotype
Bcl-2

# Figure S1

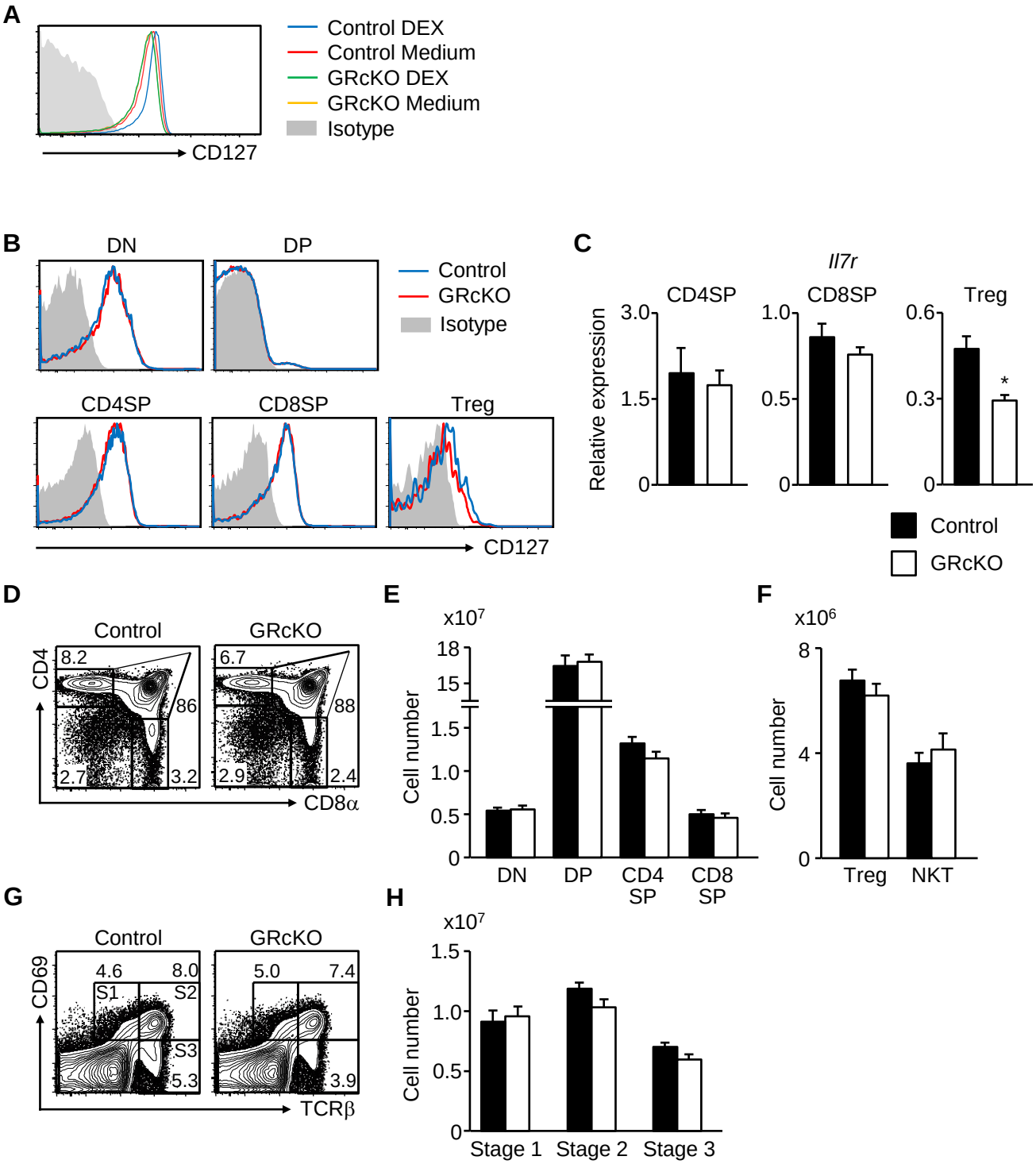
A
Control DEX
Control Medium
GRcKO DEX
GRcKO Medium
Isotype
CD127
B
DN
DP
CD4SP
CD8SP
Treg
Control
GRcKO
Isotype
CD127
C
Il7r
CD4SP
CD8SP
Treg
Relative expression
3.0
1.5
0
1.0
0.5
0
0.6
0.3
0
*
Control
GRcKO
D
Control
GRcKO
CD4
8.2
86
2.7
3.2
6.7
88
2.9
2.4
CD8α
E
x10^7
18
15
1.5
1.0
0.5
0
Cell number
DN
DP
CD4 SP
CD8 SP
F
x10^6
8
4
0
Cell number
Treg
NKT
G
Control
GRcKO
CD69
4.6
8.0
S1
S2
S3
5.3
5.0
7.4
3.9
TCRβ
H
x10^7
1.5
1.0
0.5
0
Cell number
Stage 1
Stage 2
Stage 3

# Figure S2

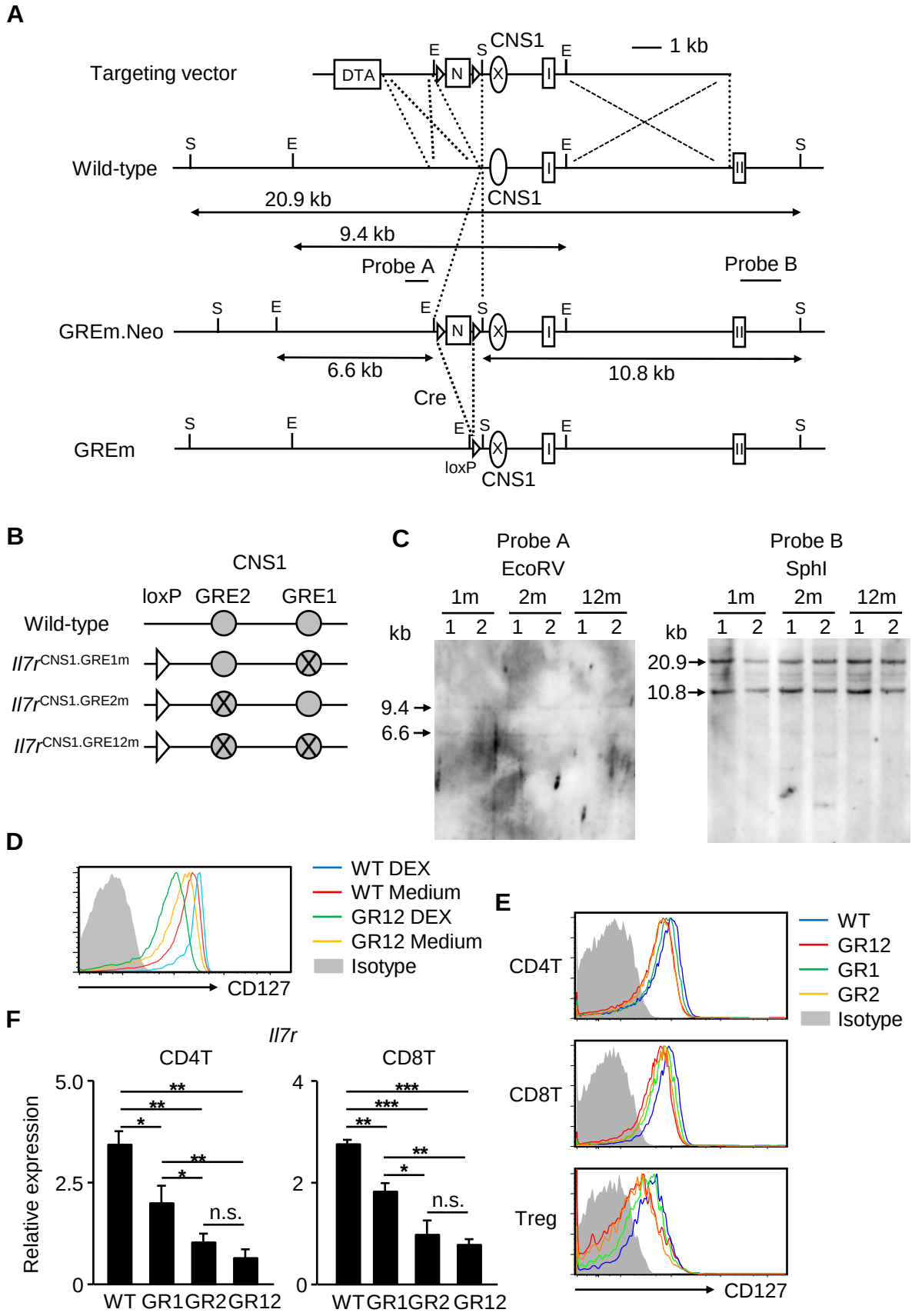
A
Targeting vector
DTA
E
N
S
CNS1
X
E
1 kb
Wild-type
S
E
E
S
20.9 kb
CNS1
9.4 kb
Probe A
Probe B
GREm.Neo
6.6 kb
10.8 kb
Cre
GREm
loxP
B
CNS1
loxP
GRE2
GRE1
Wild-type
Il7r CNS1.GRE1m
Il7r CNS1.GRE2m
Il7r CNS1.GRE12m
C
Probe A
EcoRV
Probe B
SphI
1m
2m
12m
kb
9.4
6.6
20.9
10.8
D
WT DEX
WT Medium
GR12 DEX
GR12 Medium
Isotype
CD127
E
CD4T
CD8T
Treg
WT
GR12
GR1
GR2
Isotype
CD127
F
Il7r
CD4T
CD8T
Relative expression
5.0
2.5
0
4
2
n.s.
WT GR1 GR2 GR12

# Figure S3

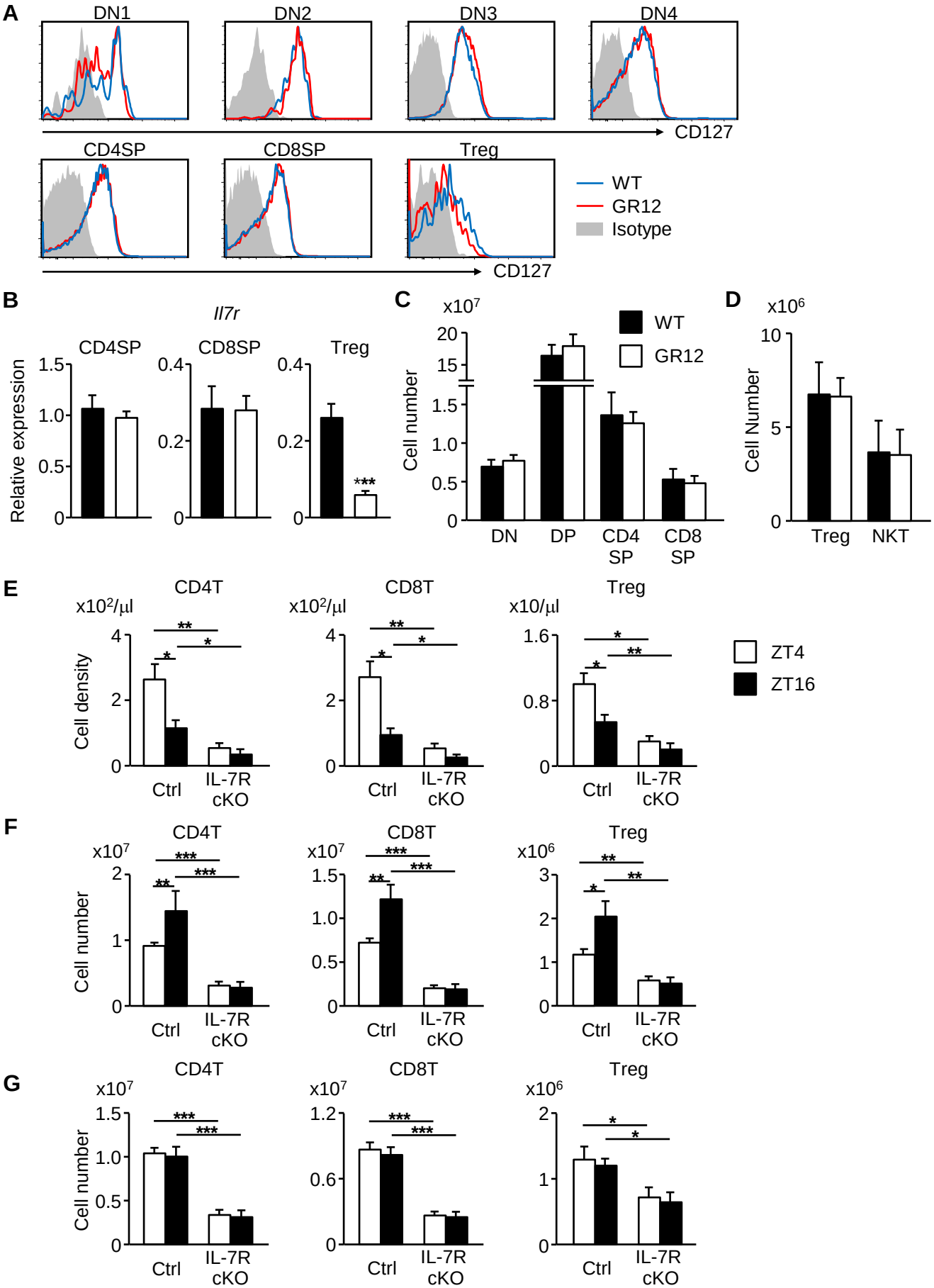
A
DN1
DN2
DN3
DN4
CD127
CD4SP
CD8SP
Treg
CD127
WT
GR12
Isotype
B
Il7r
Relative expression
CD4SP
CD8SP
Treg
***
C
x10^7
Cell number
WT
GR12
DN
DP
CD4 SP
CD8 SP
D
x10^6
Cell Number
Treg
NKT
E
CD4T
CD8T
Treg
x10^2/μl
x10^2/μl
x10/μl
Cell density
ZT4
ZT16
Ctrl
IL-7R cKO
F
CD4T
CD8T
Treg
x10^7
x10^7
x10^6
Cell number
G
CD4T
CD8T
Treg
x10^7
x10^7
x10^6
Cell number

# Figure S4

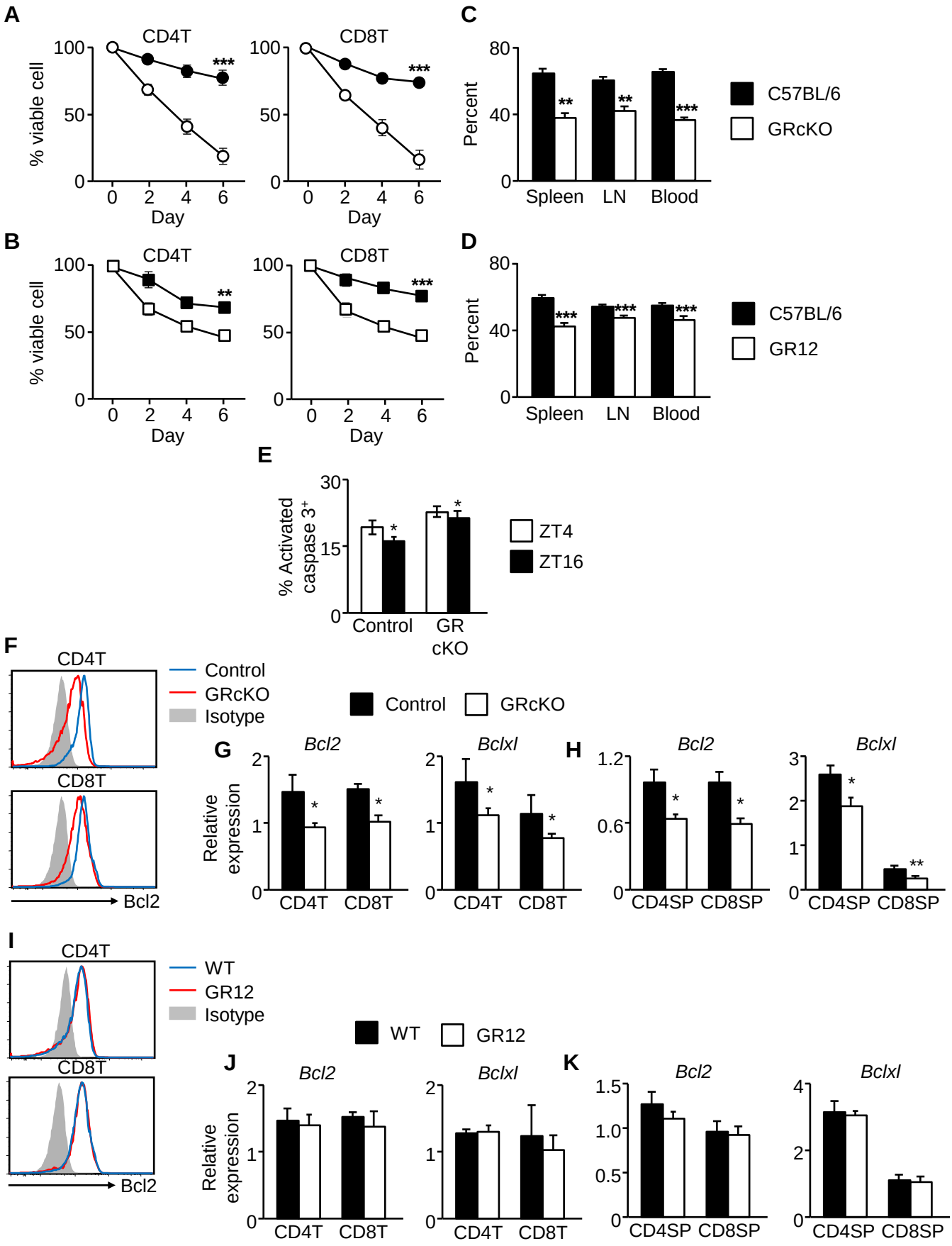
A
CD4T
CD8T
% viable cell
Day
B
C
Percent
Spleen
LN
Blood
C57BL/6
GRcKO
D
GR12
E
% Activated caspase 3+
Control
GR cKO
ZT4
ZT16
F
Control
GRcKO
Isotype
Bcl2
G
Bcl2
Bclxl
Relative expression
CD4T
CD8T
H
CD4SP
CD8SP
I
WT
GR12
J
K

# Figure S5

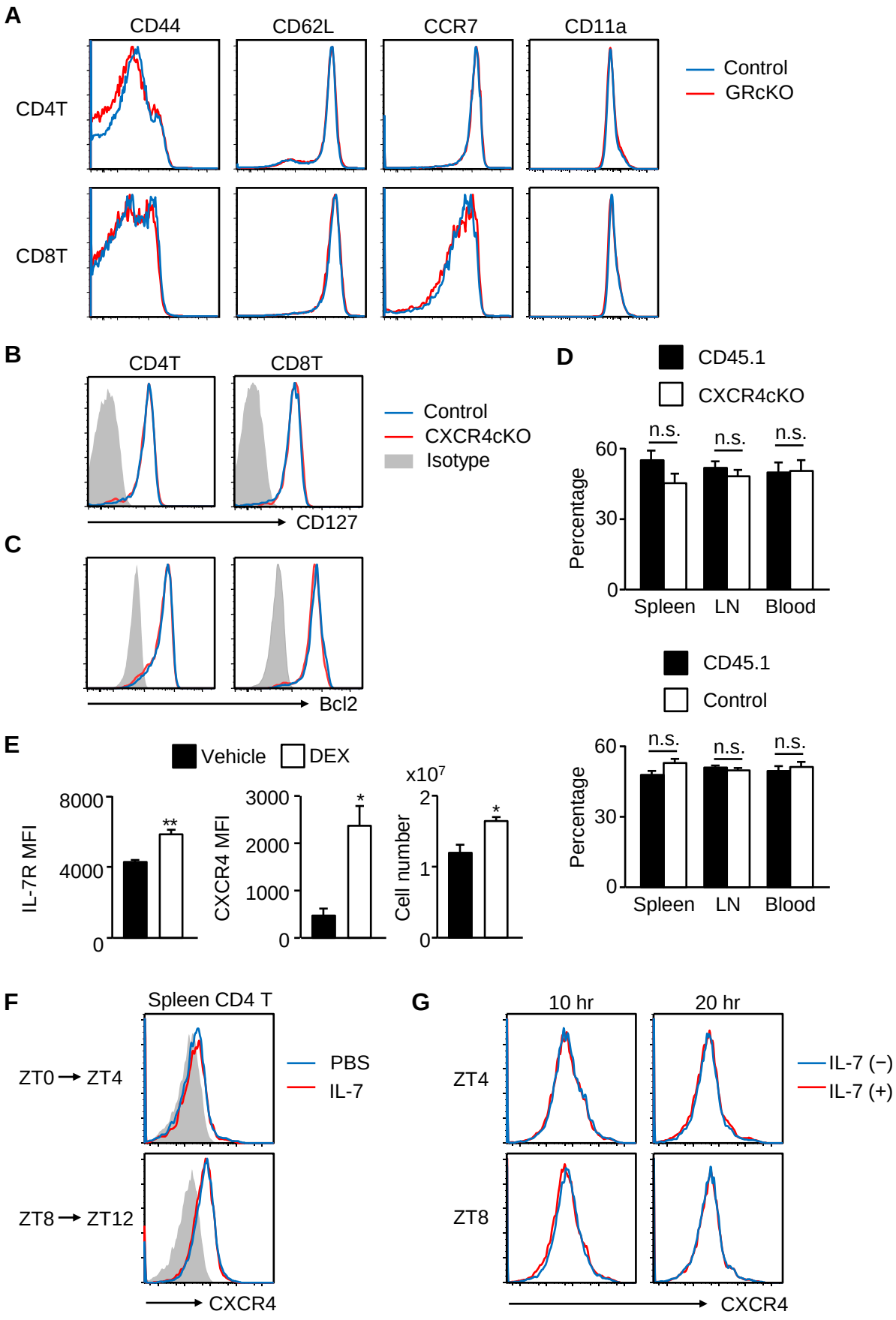
A
CD44
CD62L
CCR7
CD11a
CD4T
CD8T
Control
GRcKO
B
CD4T
CD8T
Control
CXCR4cKO
Isotype
CD127
C
Bcl2
D
CD45.1
CXCR4cKO
n.s.
Percentage
Spleen
LN
Blood
CD45.1
Control
E
Vehicle
DEX
IL-7R MFI
CXCR4 MFI
Cell number
x10^7
F
Spleen CD4 T
ZT0 → ZT4
ZT8 → ZT12
PBS
IL-7
CXCR4
G
10 hr
20 hr
ZT4
ZT8
IL-7 (−)
IL-7 (+)
CXCR4

# Figure S6

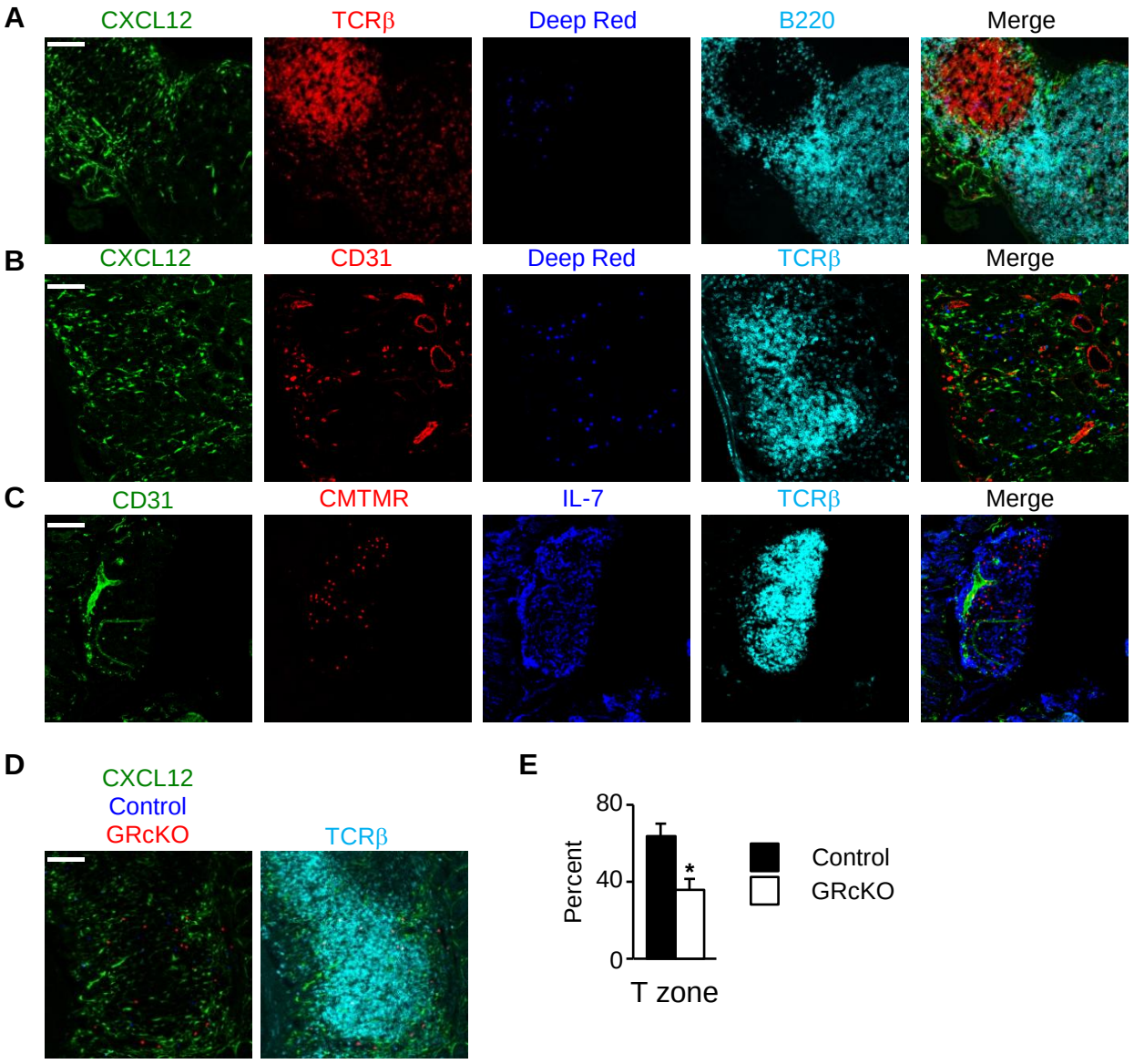
A
CXCL12
TCRβ
Deep Red
B220
Merge
B
CXCL12
CD31
Deep Red
TCRβ
Merge
C
CD31
CMTMR
IL-7
TCRβ
Merge
D
CXCL12
Control
GRcKO
TCRβ
E
80
40
0
Percent
*
Control
GRcKO
T zone

# Figure S7

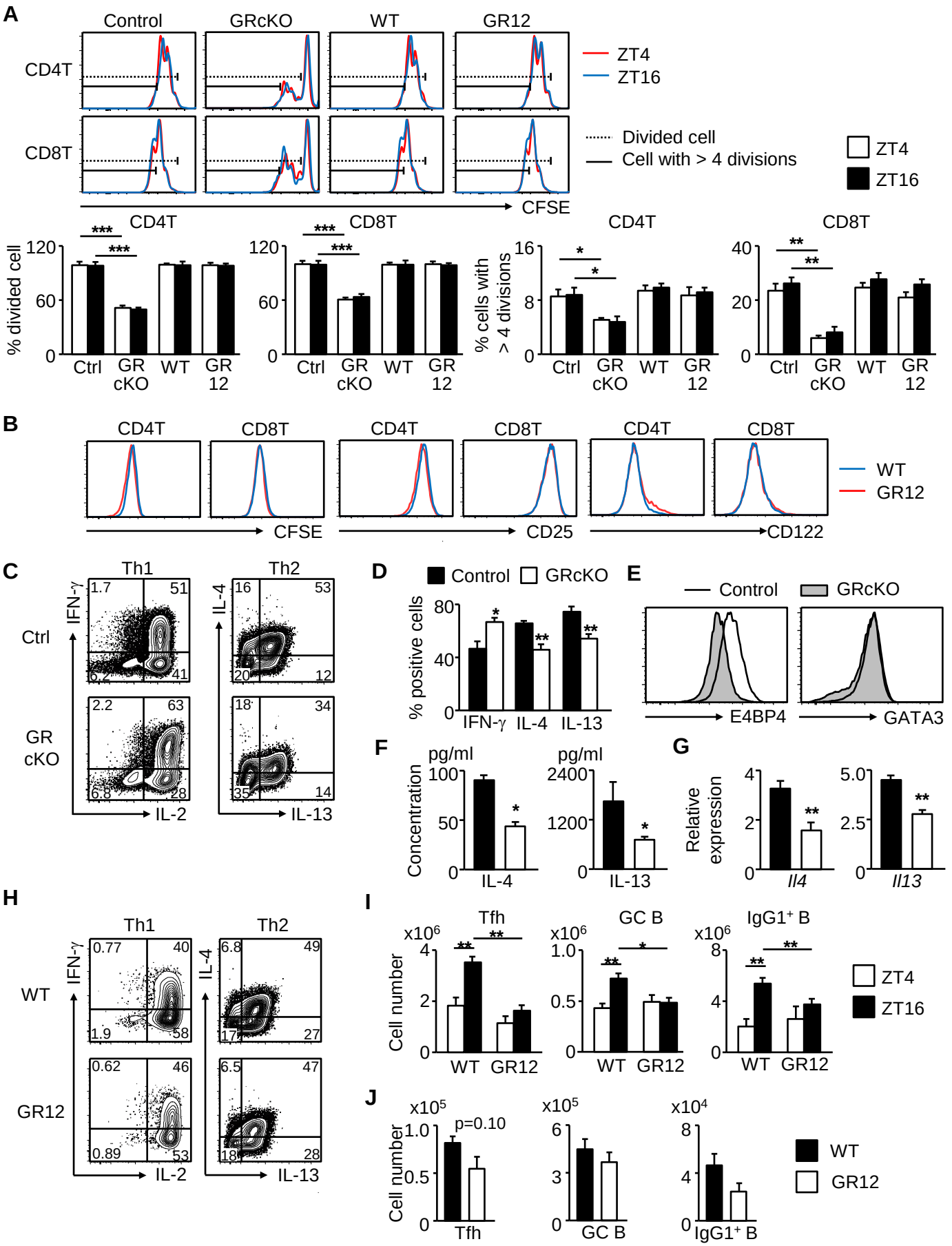
A
Control
GRcKO
WT
GR12
CD4T
CD8T
ZT4
ZT16
Divided cell
Cell with > 4 divisions
CFSE
% divided cell
% cells with > 4 divisions
Ctrl
GR cKO
GR 12
B
CD25
CD122
C
Th1
Th2
IFN-γ
IL-4
IL-2
IL-13
Ctrl
GR cKO
D
Control
GRcKO
% positive cells
IFN-γ
IL-4
IL-13
E
E4BP4
GATA3
F
pg/ml
Concentration
G
Relative expression
Il4
Il13
H
WT
GR12
I
Tfh
GC B
IgG1⁺ B
Cell number
J
p=0.10